

N O T I C E

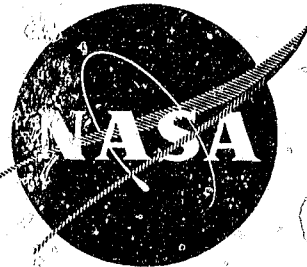
THIS DOCUMENT HAS BEEN REPRODUCED FROM
MICROFICHE. ALTHOUGH IT IS RECOGNIZED THAT
CERTAIN PORTIONS ARE ILLEGIBLE, IT IS BEING RELEASED
IN THE INTEREST OF MAKING AVAILABLE AS MUCH
INFORMATION AS POSSIBLE

✓
(NASA-CR-159697) INVESTIGATION OF CRITICAL
BURNING OF FUEL DROPLETS Final Report, 1
Sep. 1966 - 30 Jun. 1979 (Pennsylvania State
Univ.) 87 p HC A04/MF A01 CSCL 21B

N80-12142

Unclas
46156

G3/25



INVESTIGATION OF CRITICAL BURNING OF FUEL DROPLETS

FINAL REPORT

by

G. M. Faeth

Mechanical Engineering Department
The Pennsylvania State University
University Park, Pennsylvania



prepared for

NATIONAL AERONAUTICS AND SPACE ADMINISTRATION

NASA Lewis Research Center
Contract NGR 39-009-077

Richard J. Priem, Program Manager and Technical Monitor

Final Report

Under NASA Grant NGR 39-009-077

on

Investigation of Critical Burning of Fuel Droplets

by

G.M. Faeth
Department of Mechanical Engineering
The Pennsylvania State University
University Park, Pennsylvania

prepared for

National Aeronautics and Space Administration
Technical Management
NASA Lewis Research Center
Cleveland, Ohio

Dr. Richard J. Priem, Technical Officer

Investigation of Critical Burning of Fuel Droplets

Final Report

by

G.M. Faeth
Department of Mechanical Engineering
The Pennsylvania State University

SUMMARY

Three areas of research were studied, as follows:

Combustion of Bipropellant Drops. Observations were made of the combustion of drops in air, using an apparatus operating under zero-g conditions. High pressures were considered, where the drop approaches or exceeds its thermodynamic critical point during combustion. Predictions of combustion lifetime for supercritical combustion, using transient combustion models, were in good agreement with measurements. For subcritical combustion, it was found that high pressure phenomena and the solubility of combustion product gases in the liquid phase must be considered if accurate predictions of drop wet-bulb temperatures and the conditions required for critical combustion are to be obtained. Heavy hydrocarbons, burning in air, reach critical combustion conditions at pressures on the order of twice the critical pressure of the pure fuel. Light hydrocarbons tend to reach critical combustion conditions at pressures nearer their own critical pressure.

Measurements of drop combustion rates in flowing air and combustion gases were also completed. The pressure range of the experiments extended from atmospheric pressure to pressures approaching the critical combustion condition. Predictions employing constant and variable property combustion models, low and high pressure phase equilibrium models, and a correction for convection, were compared with these measurements. Burning rates were predicted with an average error of 30% using average properties in the convection correction. The major difference between the results of the low and high pressure phase equilibrium models was that the high pressure version predicts a higher pressure for supercritical combustion - in better agreement with the measurements. The use of constant or variable property gas phase models had little impact on the results, as long as any constant property was selected at an arithmetic average condition.

Combustion of Hydrazine Fuels. The combustion of hydrazine and its derivatives as drops was studied in combustion gas environments at atmospheric pressure. When oxygen is present in the gas around the drop a hybrid flame structure is observed, with an inner decomposition flame, near the surface, surrounded by an oxidation zone.

A simplified model of this process was developed which was capable of correlating the data of this and other studies, with average errors less than 20%.

The combustion response of hydrazine to imposed pressure oscillations was investigated both theoretically and experimentally in a strand burning apparatus. The theory was developed as a perturbation analysis with the zero-order results yielding mean combustion characteristics and the first-order results yielding the linear combustion response. The measurements indicated linear response for pressure oscillation amplitudes less than 15%. The analysis gave good predictions of both steady combustion and combustion response characteristics, correctly predicting both the magnitude and phase of the burning rate response. Both liquid and gas phase transient effects were considered in the analysis. The results indicate that interactions between the combustion process and liquid phase transient effects are most important for conventional combustion processes with hydrazine. Response levels sufficient to drive combustion instability were found.

The strand results were theoretically extended to the more practical case of drops and sprays. It was found that the response of monopropellant hydrazine drops and sprays can exceed unity for drop sizes, operating conditions and frequencies representative of high frequency combustion instability. The response is greatest for large drops, having mean temperature gradients, at high pressures. Response factors were less than unity for drops at their wet-bulb state. The response of a monodisperse spray is less than the response of the injected drop-size due to the reduced response of small drops near the end of their lifetime. Response of polydisperse sprays depends strongly on the initial drop size distribution; however, even a small percentage of large drops can provide appreciable response.

Combustion of Sprays. A spray combustion model was developed and systematically evaluated employing a sequence of experiments as follows: constant density jet, variable density jet, evaporating spray, combusting jet and combusting spray. The experimental conditions involved jets or two-phase flows in a stagnant environment. Measurements at atmospheric pressure consisted of mean and turbulent velocities, using the laser Doppler anemometer; mean temperatures, using fine wire thermocouples; mean composition, using isokinetic sampling and analysis by gas chromatography; and drop size distributions, using a particle impaction method. Data at elevated pressures consisted of photographs of spray and flame boundaries. Test pressures extended to supercritical conditions.

The theoretical model was based on the assumption of locally homogeneous flow (LHF) for the two-phase flows. This assumption implies that local gas and liquid velocities are the same and that the phases are in thermodynamic equilibrium, at each point in the flow. Flow characteristics were based on a k - ϵ - g turbulence model. Under these assumptions, the various flows only differ by their equation of state, which relates local mixture fraction to other properties in the flow, e.g. density, temperature, composition, etc.

Using a well-established set of turbulence model constants, the model predictions were in excellent agreement with the measurements for all single-phase flows, both noncombusting and combusting. The model provided a useful qualitative picture of the flow in evaporating and combusting sprays at atmospheric pressure (maximum errors in mean velocity and mean mixture fraction were in the range 20%) for sprays having a Sauter mean diameter on the order of 30 μm . The errors result from effects of slip and loss of thermodynamic equilibrium between the phases. Analysis of drop-life histories suggested that a Sauter mean diameter less than 10 μm would be required for quantitative accuracy at the atmospheric pressure test conditions. The comparison between theory and experiment was improved at high pressures, although additional experimental evaluation is needed in order to obtain a more definitive evaluation.

The advantage of the LHF model is that detailed information on spray conditions are not needed for a prediction. Effects of slip and loss of thermodynamic equilibrium cause the LHF model to overestimate the rate of flow development, thus the model represents a lower bound for all possible sprays. Given the predictions of the LHF model, the potential importance of slip, etc. can be assessed by completing drop-life history calculations, using the LHF results to specify the local environment of drops in the spray.

Acknowledgements

The financial support of the National Aeronautics and Space Administration, under Grant Number NGR 39-009-077, with Dr. R.J. Priem of the Lewis Research Center serving as Technical Officer, is gratefully acknowledged.

The author also wishes to acknowledge the assistance of D.P. Dominicis, R.S. Lazar, C.B. Allison, the late G.S. Canada, S.P. Chanin, A.J. Shearer, C-P. Mao and G.A. Szekely, Jr. All of these individuals contributed significantly to carrying out this investigation.

TABLE OF CONTENTS

	<u>Page</u>
SUMMARY	i
ACKNOWLEDGEMENTS	iv
LIST OF TABLES	vi
LIST OF FIGURES	vii
NOMENCLATURE	x
I. INTRODUCTION	1
II. COMBUSTION OF BIROPELLANT DROPS	1
2.1 Introduction	1
2.2 Supercritical Drop Combustion	2
2.3 High Pressure Drop Combustion	6
2.3.1 Zero-Gravity Combustion	6
2.3.2 Combustion under Convection Conditions	12
III. COMBUSTION OF HYDRAZINE FUELS	23
3.1 Introduction	23
3.2 Steady Drop Combustion	23
3.3 Combustion Response of Liquid Hydrazine Fuels	28
3.3.1 Liquid Strand Combustion	28
3.3.2 Drop and Spray Combustion	32
IV. COMBUSTION OF SPRAYS	41
4.1 Introduction	41
4.2 Spray Evaporation	42
4.3 Spray Combustion	56
REFERENCES	67

LIST OF TABLES

<u>Table No.</u>	<u>Title</u>	<u>Page</u>
1	Measured and Predicted Pressures for Supercritical Droplet Combustion in Air	11
2	Summary of Test Conditions for Drop Combustion Rates in Combustion Gas Environments	22
3	Summary of Test Conditions for Drop Combustion Rates of Hydrazine Fuels	27
4	Frequency Ranges for Potentially Unstable Combustion of Hydrazine	36
5	Summary of Test Conditions	45
6	Constants in the Turbulence Model	49
7	Summary of Test Conditions for Combusting Jets at Atmospheric Pressure	58
8	Summary of Test Conditions for Combusting Sprays in High Pressure Air	60
9	Comparison of Measured and Predicted Spray Penetration Lengths for Combusting Sprays at High Pressures	65

LIST OF FIGURES

<u>Figure</u>	<u>Caption</u>	<u>Page</u>
1	Sketch of the zero-gravity test chamber	4
2	Droplet temperature measurements for n-decane in air at various pressures. Pressures and initial drop diameters: Curve A, 0.79 MPa, 945 μm ; Curve B, 3.55 MPa, 990 μm ; Curve C, 7.58 MPa, 947 μm	5
3	Supercritical combustion lifetimes for n-decane at 6.89 MPa as a function of stoichiometry parameter, initial diameter corrected to 875 μm .	7
4	Theoretical and experimental steady-burning temperatures for n-octane droplets burning in air under zero-gravity conditions	9
5	Predictions of droplet-surface fuel mole fractions as a function of liquid temperature for n-decane evaporating in nitrogen at 3000 K . . .	10
6	Sketch of the flat flame burner apparatus	14
7	Sketch of the high pressure burner apparatus . .	15
8	Theoretical and experimental drop burning rates for various paraffins in a flowing combustion gas environment at atmospheric pressure: Gas velocity, 0.625 m/s; gas temperature, 2530 K; drop diameter, 1100 μm	16
9	Porous sphere burning rates of paraffins in air, for fuel inlet and ambient temperatures of 300 K. Sphere diameter, 9.5 mm	18
10	Overall comparison of theoretical and experimental gasification rates in combustion gas environments. Lines A-A are data bounds when average properties are used in the convection correction	20
11	Predicted liquid-surface compositions for porous sphere combustion. Ambient temperature 1145K. Fuel inlet temperature 300K	21
12	Hydrazine burning rate as a function of drop diameter for a typical oxidation condition . . .	25
13	Comparison of predicted and measured burning rates for hydrazine	26

<u>Figure</u>	<u>Caption</u>	<u>Page</u>
14	Sketch of the oscillatory strand combustion apparatus	29
15	Theoretical and experimental steady hydrazine strand burning rates as a function of pressure .	31
16	Theoretical and experimental magnitude of the liquid surface oscillation of burning hydrazine as a function of the frequency of the imposed pressure oscillation	33
17	Theoretical and experimental phase angle of the liquid surface oscillation of burning hydrazine as a function of the frequency of the imposed pressure oscillation	34
18	Predicted real-part of the acoustic admittance for hydrazine strand combustion	35
19	Predicted hydrazine droplet response as a function of frequency and size	39
20	Predicted response of a polydisperse hydrazine spray as a function of frequency	40
21	Schematic diagram of the LDA system for jet and spray measurements	44
22	Equation of state for an evaporating Freon-11 spray	48
23	Theoretical and experimental radial variation of mean axial velocity for constant and variable density gas jets and an evaporating spray	50
24	Theoretical and experimental radial variation of Reynolds stress for constant and variable density gas jets and an evaporating spray	52
25	Theoretical and experimental variation of mean centerline velocity for various gas jets and an evaporating spray	53
26	Theoretical and experimental variation of mean centerline mixture fraction for various gas jets and an evaporating spray	54
27	Predicted drop-life histories in an evaporating spray	55

<u>Figure</u>	<u>Caption</u>	<u>Page</u>
28	Sketch of the high pressure spray combustion apparatus	59
29	Equation of state for a combusting n-pentane spray in air at 6 MPa	62
30	Theoretical and experimental mean velocity and temperature variation along the centerline of a combusting gas jet at atmospheric pressure . .	63
31	Theoretical and experimental mean velocity and temperature variation along the centerline of a combusting spray at atmospheric pressure . . .	64

NOMENCLATURE

<u>Symbol</u>	<u>Description</u>
a	gravitational acceleration
A	Damkohler number
C_i	constants in turbulence model
d	injector passage diameter
D	drop diameter
E	activation energy, dimensionless activation energy
f	mixture fraction
g	square of mixture fraction fluctuations
k	turbulence kinetic energy
K	burning rate constant
\dot{m}_0	injector mass flow rate
\dot{M}	jet momentum
n	reaction order
P	pressure
P_r	reduced pressure, drop response factor
P_{rf}	spray response factor
r	mass of oxidant per unit mass of fuel for stoichiometric combustion, radial distance
t	time
T	temperature
u	axial velocity
v	radial velocity
v^0	effective radial velocity, Eq. (6)
x	axial distance
Y_i	mass fraction of species i
ϵ	dissipation rate of turbulent kinetic energy

μ_t	turbulent viscosity
ν	stoichiometry parameter
ρ	density
σ	turbulent Prandtl/Schmidt number
χ	transport parameter
ω	dimensionless frequency

Subscripts

A	air
C	centerline
F	injected fluid
Ff	injected fluid in liquid phase
Fg	injected fluid in gas phase
i	initial state
o	initial state
X	oxygen
∞	ambient state
∞_0	steady flame condition

Superscripts

—	mean quantity
'	fluctuating quantity

I. INTRODUCTION

This investigation considers aspects of the general problem of spray combustion. The research was primarily motivated by a need for better understanding of stable and unstable combustion in liquid-fueled rocket engines. However, the results also have application to other liquid-fueled combustion systems, e.g., gas turbines, furnaces and Diesel engines.

Three areas of research were studied under the grant:

1. Combustion of bipropellant drops. In this area, particular emphasis was placed on high pressure combustion of individual drops, under conditions where the liquid drop approaches or exceeds its thermodynamic critical point. Theory was developed to assist the interpretation of experimental results and to establish methods for computing drop behavior for conditions that were not explicitly tested. The measurements involve pure hydrocarbon and alcohol fuels, in air and combustion gas environments, at pressures up to 13.8 MPa (2000 psia).
2. Combustion of hydrazine fuels. Combustion of hydrazine, MMH and UDMH as drops was studied both theoretically and experimentally. This involved basic measurements of combustion rates of drops in combustion gas environments, and modeling the process to include both decomposition and oxidation phenomena. The combustion response of liquid hydrazine to imposed pressure oscillations was also studied. Predicted and measured response for burning hydrazine strands were compared. Based on these results, predictions of drop and spray response were obtained.
3. Combustion of sprays. The final stages of the investigation considered the development of a model for spray combustion and obtaining experimental results to evaluate this model. High pressure conditions where phenomena associated with the liquid approaching its thermodynamic critical point are significant was considered as well as low pressure operation. The model was evaluated systematically considering: constant density jets, variable density jets, combusting jets, evaporating sprays, and combusting sprays.

In this report, each area of the research is briefly described, and the major findings are discussed. Further details may be found in specific reports (1-18)*, papers (19-38) and theses (39-49) resulting from this grant.

II. COMBUSTION OF BI-PROPELLANT DROPS

2.1 Introduction

A central problem that must be resolved prior to any rational treatment of spray combustion involves the transport characteristics

*Numbers in parenthesis denote references.

of individual drops within a spray. This phase of the investigation was concerned with processes of heat and mass transfer to individual drops. A variety of test conditions were examined; however, the main emphasis was placed on hydrocarbon and alcohol fuels, in combustion gas environments at high pressures (where operation near the thermodynamic critical point of the fuel must be considered).

Two topics were considered in this portion of the research, as follows:

1. Supercritical drop combustion. This topic involves conditions where the drop exceeds its thermodynamic critical point, and burns in a transient manner, similar to a puff of gas. Experiments were conducted to observe drop combustion under these conditions. The measurements were compared with theoretical results in the literature.
2. High pressure drop combustion. This area involved the determination of the pressure levels required for supercritical combustion, and heat and mass transfer rates in the near critical pressure regime. Theory was developed for these parameters, and compared with the measurements.

The main results obtained in each of these areas is described in the following sections.

2.2 Supercritical Drop Combustion

Introduction. Theoretical investigations by Spalding (50), Wieber (51), Brzustowski (52) and Rosner (53) indicated that at sufficiently high pressures, a fuel drop can exceed its thermodynamic critical point during combustion. When this occurs, the quasisteady drop combustion theories, employed with good success to predict liquid-fueled rocket engine performance at moderate pressures (54), no longer represent the combustion process and a new burning regime must appear. The pressure regime for this behavior is in the range of operation of some liquid-fueled rocket engines and Diesel engines. Some modern, high pressure ratio gas turbine combustors approach this region of operation as well.

Upon reaching its thermodynamic critical point, a droplet becomes a puff of gas. Spalding (50) theoretically considered combustion in this case by approximating the droplet vapor as an instantaneous point source of fuel. Laminar combustion and spherical symmetry were assumed in the analysis. The flame was taken to be infinitely thin, with fuel and oxidant combining in stoichiometric proportions. Physical properties were assumed to be constant. Rosner (53), modified Spalding's analysis to account for the initially finite dimensions of the fuel vapor pocket.

Both these analyses, and the theories used to suggest the onset of critical combustion, contain many approximations. Therefore, the main objective of the present investigation was to obtain experimental

results to test the predictions. Only a limited description of the investigation is presented here, further details can be found in Refs. 1-3, 19-21, 39 and 41.

Apparatus. A sketch of the test apparatus appears in Fig. 1. The apparatus consisted of a pressure vessel fitted with windows to allow motion pictures of the combustion process. A drop was supported at the center of the chamber on either a quartz fiber or a thermocouple junction. The drop was ignited with a hot wire. The gaseous environment of the drop consisted of various mixtures of oxygen and nitrogen.

As the critical point of a drop is approached, surface tension approaches zero, and the supported drop technique is not feasible since the drop would fall from the probe. This problem was avoided by conducting the experiment in a freely falling apparatus, which provided a test time of approximately 1s under nearly zero-gravity conditions. Data was obtained on drop temperature and flame shape variations during combustion, as well as the time for complete combustion.

Results and Discussion. Figure 2 is an illustration of drop temperature variation as a function of time after ignition at various pressures. The inflection of the temperature trace a short time after ignition corresponds to the point when the thermal disturbance due to the presence of a flame propagates to the thermocouple position.

At lower pressures, curve A of Fig. 2, the temperature of the drop levels out at the wet bulb temperature (the condition where all the heat transferred from the flame to the drop is utilized for the heat of vaporization of the evaporating fuel). The temperature then rises again after all the liquid is gone. This behavior is characteristic of subcritical combustion, treated by the vaporization controlled models(54).

As the pressure is increased, curve B of Fig. 2, the time spent at the wet bulb state decreases. Eventually, a condition is reached where the drop temperature increases continuously, curve C. This is indicative of supercritical combustion, which persists for all higher pressures. In this case, the fuel becomes gradually more vapor-like as its temperature increases and the bulk of the liquid does not evaporate from a liquid surface as it does at low pressures.

Tests were conducted under supercritical combustion conditions and measurements were made of the time of combustion, for comparison with the theories of Refs. 50 and 53. A portion of these results is illustrated in Fig. 3. Combustion lifetime, corrected to a fixed initial drop size, is plotted as a function of a stoichiometric factor,

$$v = Y_X/r$$

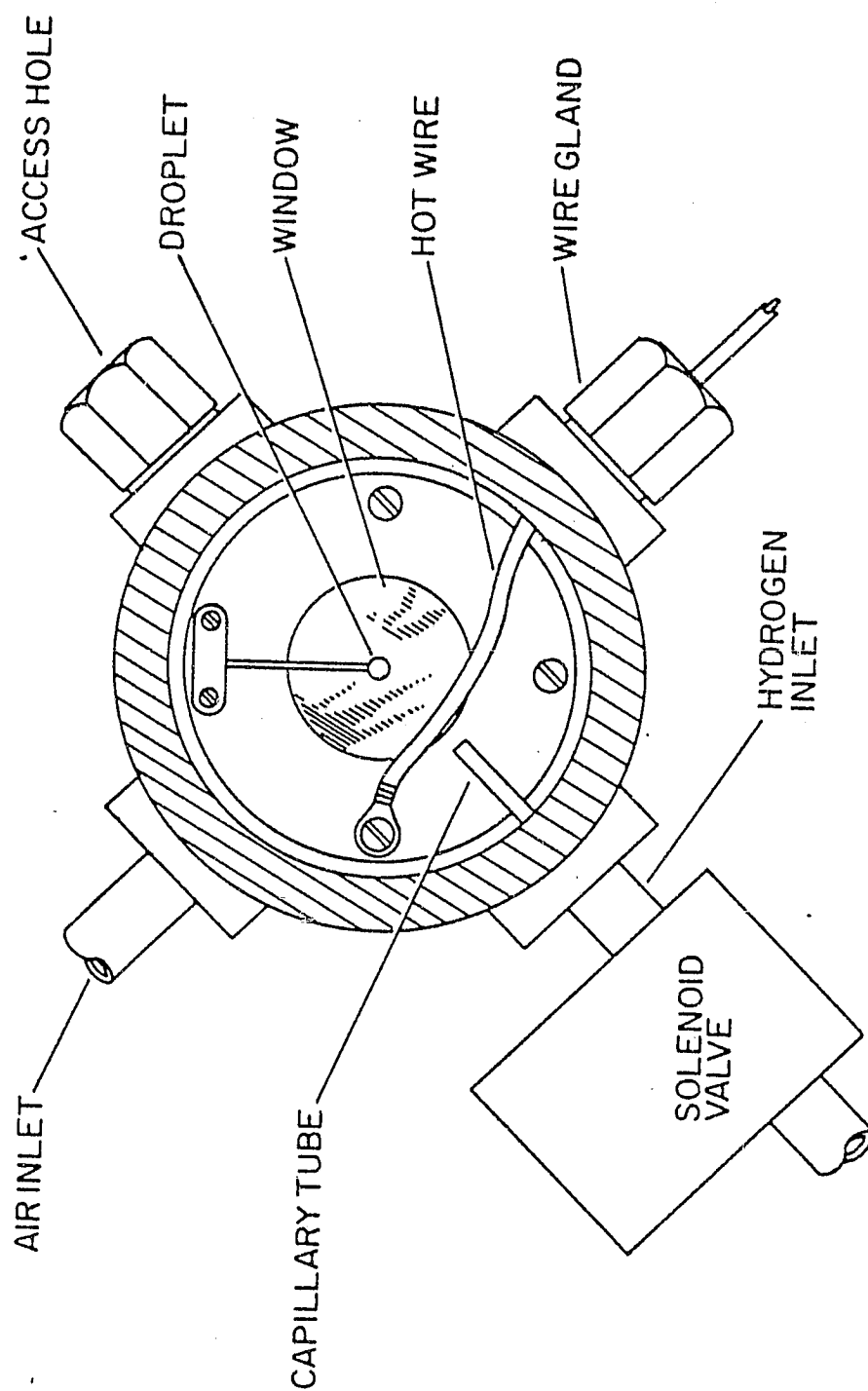


Fig. 1 Sketch of the zero-gravity test chamber.

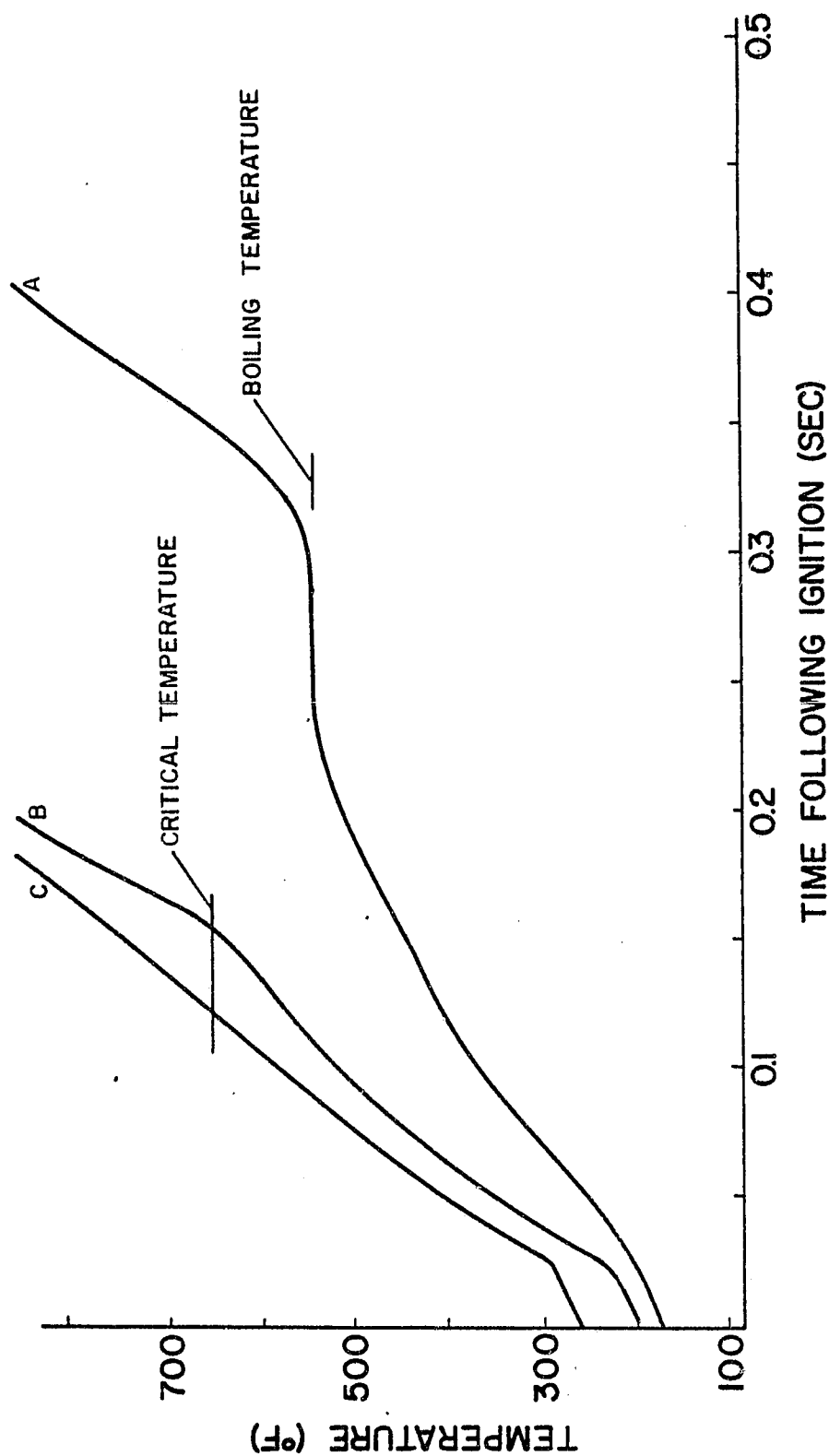


Fig. 2 Droplet temperature measurements for n-decane in air at various pressures. Pressures and initial drop diameters: Curve A, 0.79 MPa, 945 μm ; Curve B, 3.55 MPa, 990 μm ; Curve C, 7.58 MPa, 947 μm .

where Y_∞ is the ambient oxident concentration and r is the mass of oxident required to consume a unit mass of fuel. The difference between the two theories is not large for the test range of Fig. 3. The experimental results are in good agreement with predictions.

Other factors, such as initial drop size, flame shape and total pressure, were also examined during the study. The predictions were satisfactory with respect to these variables as well.

Conclusions. This study provided the first experimental observations of supercritical combustion of individual drops. No unusual change in the structure of the combustion zone was observed as the drop passed through its critical condition. In general, predictions of the two theoretical models were in reasonably good agreement with the observations.

2.3 High Pressure Drop Combustion

2.3.1 Zero-Gravity Combustion

Introduction. With supercritical combustion resolved, at least in the absence of forced convection, attention turned to determining the conditions required for supercritical combustion to appear. Wieber (51) had earlier computed total pressures required for supercritical evaporation of oxygen and n-heptane drops in a high temperature inert gas. However, this analysis did not allow for the influence of high pressures on the thermodynamic properties of the fuels, and particularly, the increased solubility of liquid fuels for combustion gases at high pressures. Manrique and Borman (55) suggested that these effects have a significant influence on drop equilibrium conditions at high pressures.

In the light of these findings, high pressure drop combustion was considered both theoretically and experimentally. Emphasis was placed on determining wet-bulb temperatures during subcritical drop combustion. Complete details of this portion of the study can be found in Refs. 4-6, 21-24, and 41.

Apparatus. The apparatus was essentially the same as described in Section 2.2. Drop temperatures were measured with thermocouples constructed of 25, 50 and 75 μm wires. Results with the smallest wires suggested that errors were small using 50 μm wires and these were employed for the bulk of the tests.

Theory. A theoretical model for the combustion process at high pressures was developed. There are two aspects to the model, a gas phase combustion model and a model for phase equilibrium at the drop surface.

The gas phase combustion model was an extension of the quasisteady drop burning model of Goldsmith and Penner (56). This model assumes spherical symmetry, quasisteady combustion at the wet-bulb state and

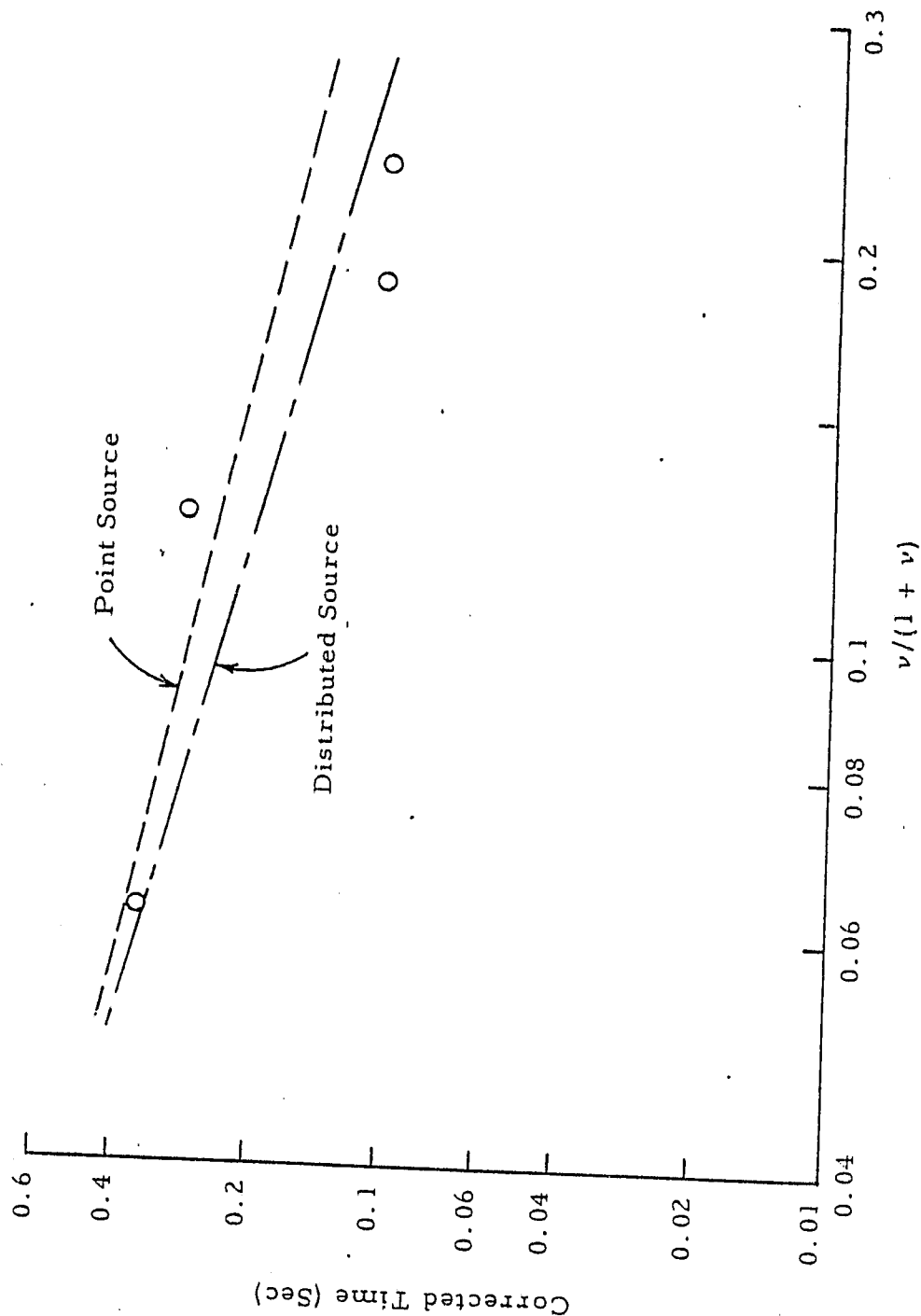


Fig. 3 Supercritical combustion lifetimes for n-decane at 6.89 MPa as a function of stoichiometry parameter, initial diameter corrected to 875 μm .

an infinitely thin diffusion flame. The model provides for variable properties in the gas phase. The extension completed in this investigation involved consideration of the effect of dissolved gas evaporation, separate determination of the concentrations of various gas phases species, and allowing for variable specific heats of all species.

Two models were employed for computing phase equilibrium conditions at the surface of the drop. The simplest model corresponded to the usual treatment of phase equilibrium, valid only at low pressures (54). The second model provided for solubility and high pressure effects, using a modified Redlich-Kwong equation of state developed by Prausnitz and Chueh (57).

Results and Discussion. Figure 4 is an illustration of predicted and measured wet-bulb temperatures as a function of pressure for the combustion of n-octane drops in air. The boiling curve, and the predictions from the low and high pressure phase equilibrium model are shown on the figure. Uncertainty bands are indicated on the theoretical results. Greatest uncertainties were due to a transport parameter χ_F , which is not known very accurately. The theoretical curves are terminated where steady burning solutions no longer exist. The experimental results are terminated when an inflection could no longer be observed in the plot of drop temperature variation with time, c.f. Fig. 2. The supercritical region occurs at pressures higher than this, and follows the unsteady combustion mechanism described in Section 2.2.

The high pressure model is in reasonably good agreement with the measurements in Fig. 4, both with respect to the wet-bulb temperature and the pressure range required for supercritical combustion. The low pressure theory underestimates the pressure required for critical combustion by roughly a factor of 2.

Measured and predicted pressures for supercritical combustion are summarized in Table 1 for n-pentane, n-octane and n-decane. The high pressure theory provides the best prediction of supercritical combustion pressure. It is also seen that the critical combustion pressure tends to approach the critical pressure of the pure fuel as the molecular weight of the fuel decreases.

The general characteristics of steady evaporation at high pressures are illustrated in Fig. 5. The plot illustrates the locus of steady evaporation states from the gas phase model and the locus of phase equilibrium states from the phase equilibrium theory. The two loci yield fuel mole fractions in the gas phase at the liquid surface, as a function of liquid temperature, with reduced pressure as a parameter. As a droplet heats-up, after ignition, it follows the locus of phase equilibrium states. At the point where the two loci intersect, drop heating ceases, and the steady evaporation period of the drop begins. As the pressure is increased, a condition is reached where the two loci are just tangent. This is the highest pressure where steady evaporation

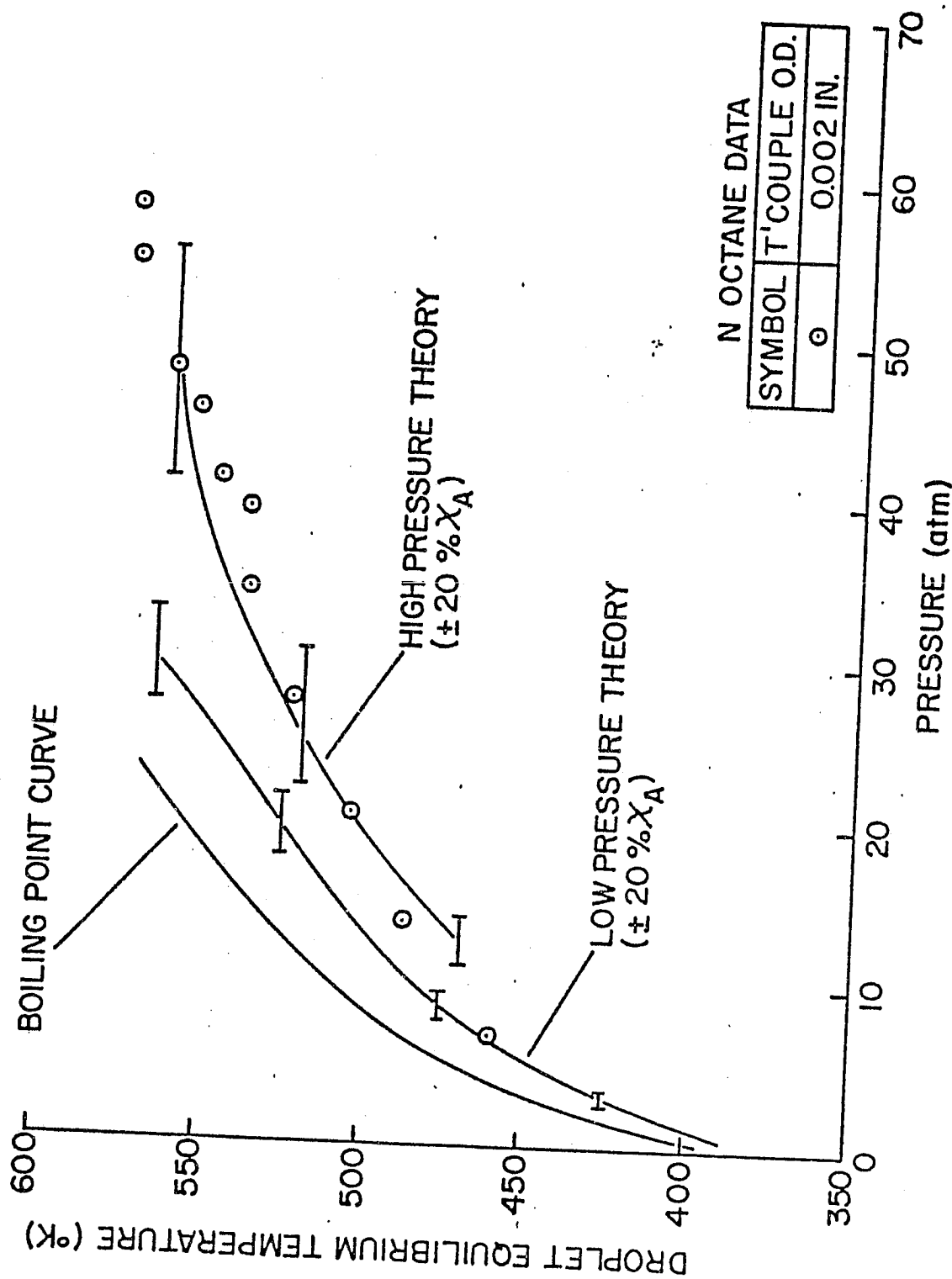


Fig. 4 Theoretical and experimental steady-burning temperatures for n-octane droplets burning in air under zero-gravity conditions.

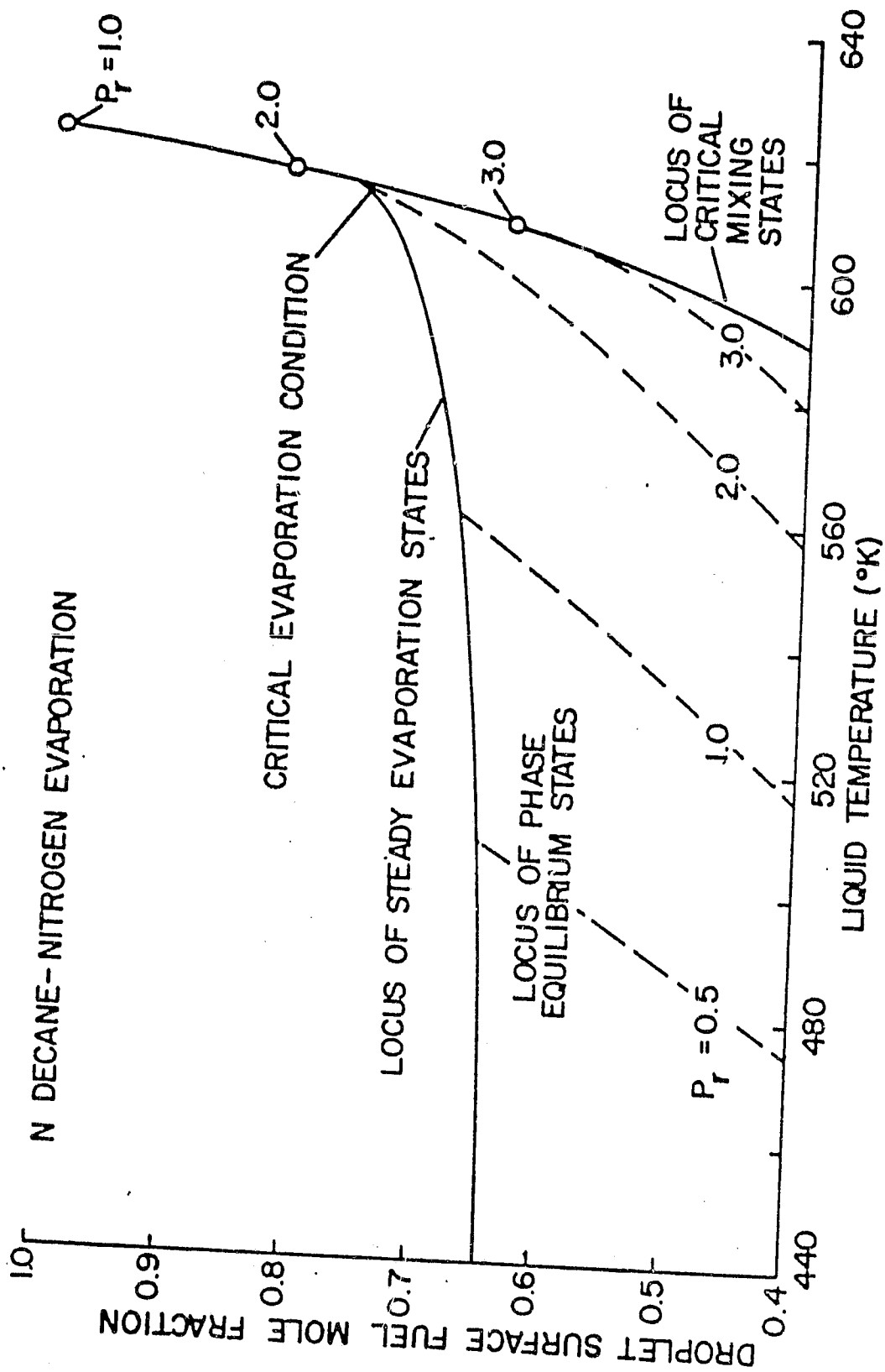


Fig. 5 Predictions of droplet-surface fuel mole fractions as a function of liquid temperature for n-decane evaporating in nitrogen at 3000 K.

Table 1

Measured and Predicted Pressures Required for Supercritical Combustion

Fuel	n-Pentane	n-Octane	n-Decane
Measured critical burning pressure (atm)	-	58-61	44-47
Measured critical P_r^a	-	2.4-2.5	2.1-2.3
Predicted critical P_r , low pressure theory ^b	1.1-1.2	1.2-1.4	1.2-1.5
Predicted critical P_r , high pressure theory ^b	1.2-1.7	1.7-2.3	1.8-2.8

^a $P_r = (\text{critical burning pressure}) / (\text{thermodynamic critical pressure of pure fuel})$

^b variation due to $\pm 20\%$ variation in χ_F

is observed. At this limit, the drop evaporates at a thermodynamically subcritical state. At higher pressures, heat input to the drop from the flame always exceeds the energy required to vaporize the fuel, and drop heating continues along the locus of phase equilibrium states. When the locus of critical mixing states is crossed, the material become gas-like and subsequently burning is unsteady supercritical combustion.

Conclusions. The results indicate that high pressure effects and the solubility of combustion gases in the liquid phase must be considered if accurate predictions of drop wet-bulb temperatures and the pressure required for critical combustion are to be obtained. For heavier hydrocarbons, burning in air, the critical combustion pressure is on the order of twice the critical pressure of the pure fuel. Lighter hydrocarbons, however, tend to reach critical combustion conditions at pressures nearer their thermodynamic critical pressure. Conditions were also found, at high pressures, where water vapor produced by combustion condenses on the liquid surface during the early stages of drop heat-up.

2.3.2 Combustion under Convection Conditions

Introduction. The zero-gravity experiments were useful for examining critical combustion conditions; however, attempts to obtain information on drop gasification rates were not particularly successful. The heated zone around the droplet caused excessive bending of background light beams; therefore, conventional shadowgraphs could not be employed to find the variation of drop size with time, at high pressures. Under zero-gravity conditions, the drop combustion process, even at subcritical combustion conditions, is intrinsically unsteady (34). Unsteadiness increases the difficulties of data interpretation. Finally, drop motion is a significant effect for drops in sprays and information in this area is needed.

With these problems in mind, a series of experiments were conducted in order to examine both high pressure phenomena and convection. As a baseline, tests were conducted at atmospheric pressure, with drops supported in combustion products of a flat flame burner. Subsequent tests employed the porous sphere technique, which allows unsteadiness to be eliminated. These results provided burning rates and liquid surface temperatures at pressures extending to the supercritical combustion condition. Both air and combustion gases were employed as the environment for porous sphere combustion. The experiments were compared with predictions, using models similar to those discussed in Section 2.3.1.

Complete details of this portion of the investigation can be found in Refs. 8-11, 25, 28, 30, 41, and 44.

Apparatus. Two different test arrangements were employed for the convection experiments. The supported droplet technique was employed for baseline tests at atmospheric pressure. The test arrangement in

this case is illustrated in Fig. 6. The drops were supported on a quartz filament. Combustion gas environment was provided by a flat flame burner. Various burner mixture ratios were employed to achieve a range of temperatures and oxident concentrations for the drop environment. The burner could be rapidly moved under the droplet, using a pneumatic cylinder, in order to initiate the combustion process. The variation of drop diameter with time was obtained from motion picture shadow-graphs.

The second test arrangement employed the porous sphere technique. A sketch of this apparatus appears in Fig. 7. The tests were conducted within a water-cooled pressure vessel, fitted with windows to allow observation of the combustion process. Droplets were simulated by porous spheres of various sizes. The fuel flow rate to the sphere could be varied, using a variable displacement pump. The steady combustion rate of the sphere was determined as the point where the sphere neither dripped liquid or dried-off. A system of burettes at the pump inlet was used to determine the steady burning rate. Combustion gas environments were provided by a burner housed at the bottom of the pressure vessel. Control of the ambient conditions of the sphere was similar to method employed for the flat flame burner apparatus. Tests were also conducted with the sphere in an air environment with this apparatus. In this case, a slow flow of air was maintained through the chamber in order to prevent vitiation of the air. Drop surface temperatures were measured, using 76 μ m thermocouples imbedded flush with the surface of the porous sphere.

Theory. The combustion model discussed in Section 2.3.1 was used for comparison with the present measurements. Spherical symmetry and no convection was assumed for the original model. Therefore, the effect of convection was included as correction factor, multiplying the prediction for no convection. This is a standard procedure, widely used in the mass transfer literature (34, 51, 54). The correlation used in the present work has good asymptotic properties, and properly agrees with theory at the low Reynolds number limit (34).

As in earlier work (Section 2.3.1) both the low and high pressure phase equilibrium models were employed for the predictions. For porous sphere combustion, however, the boundary condition at the liquid surface must be modified from that employed for drop combustion. This is due to the fact that the liquid entering the sphere must always be heated to the surface temperature, while bulk heating of a drop ceases during the steady evaporation period.

Results and Discussion. Some typical results of the baseline supported drop tests are illustrated in Fig. 8. Over a limited diameter range, with the drop at its wet-bulb state, the square of the drop diameter varies linearly (34)

$$\frac{dD^2}{dt} = -K$$

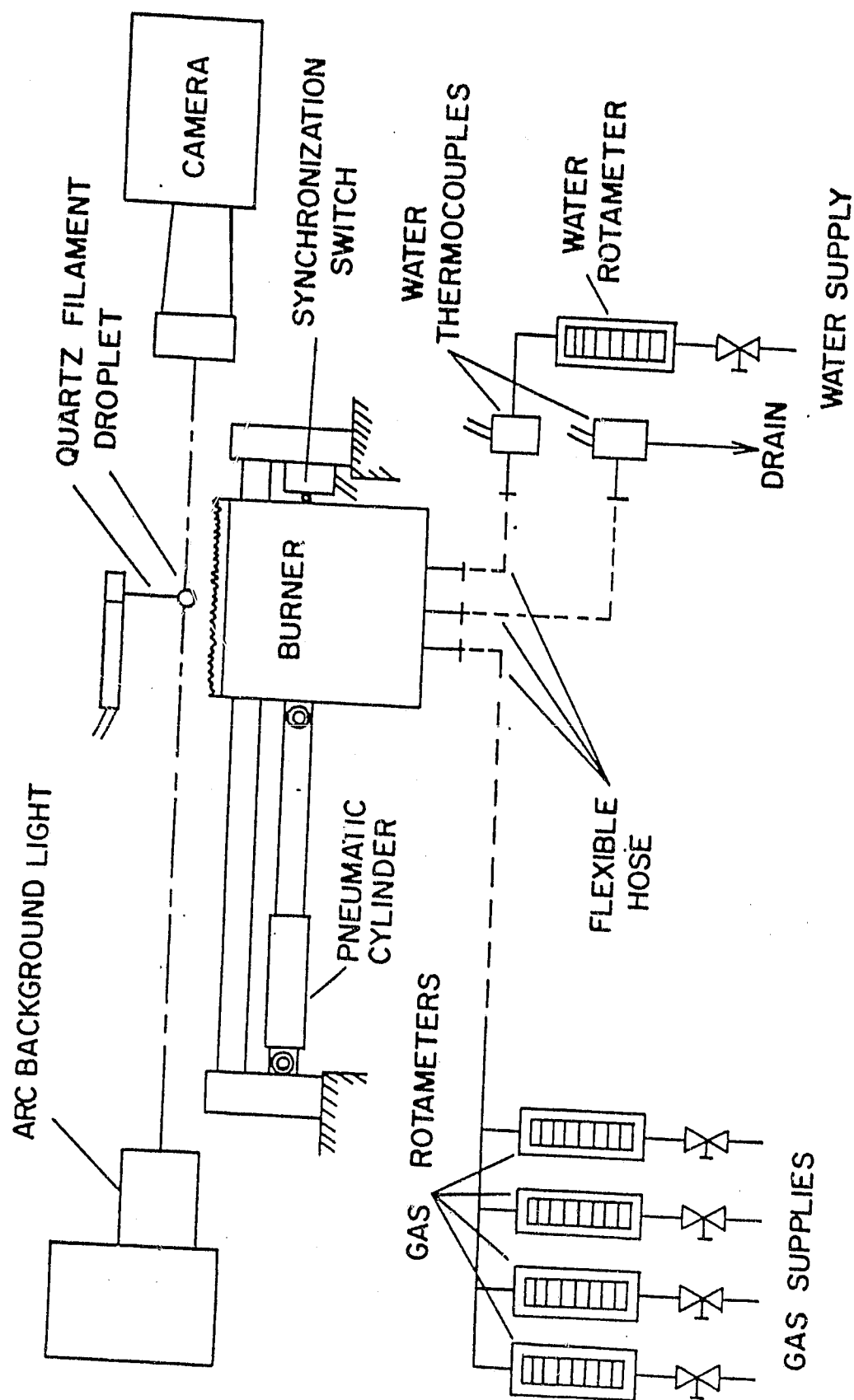


Fig. 6 Sketch of the flat flame burner apparatus.

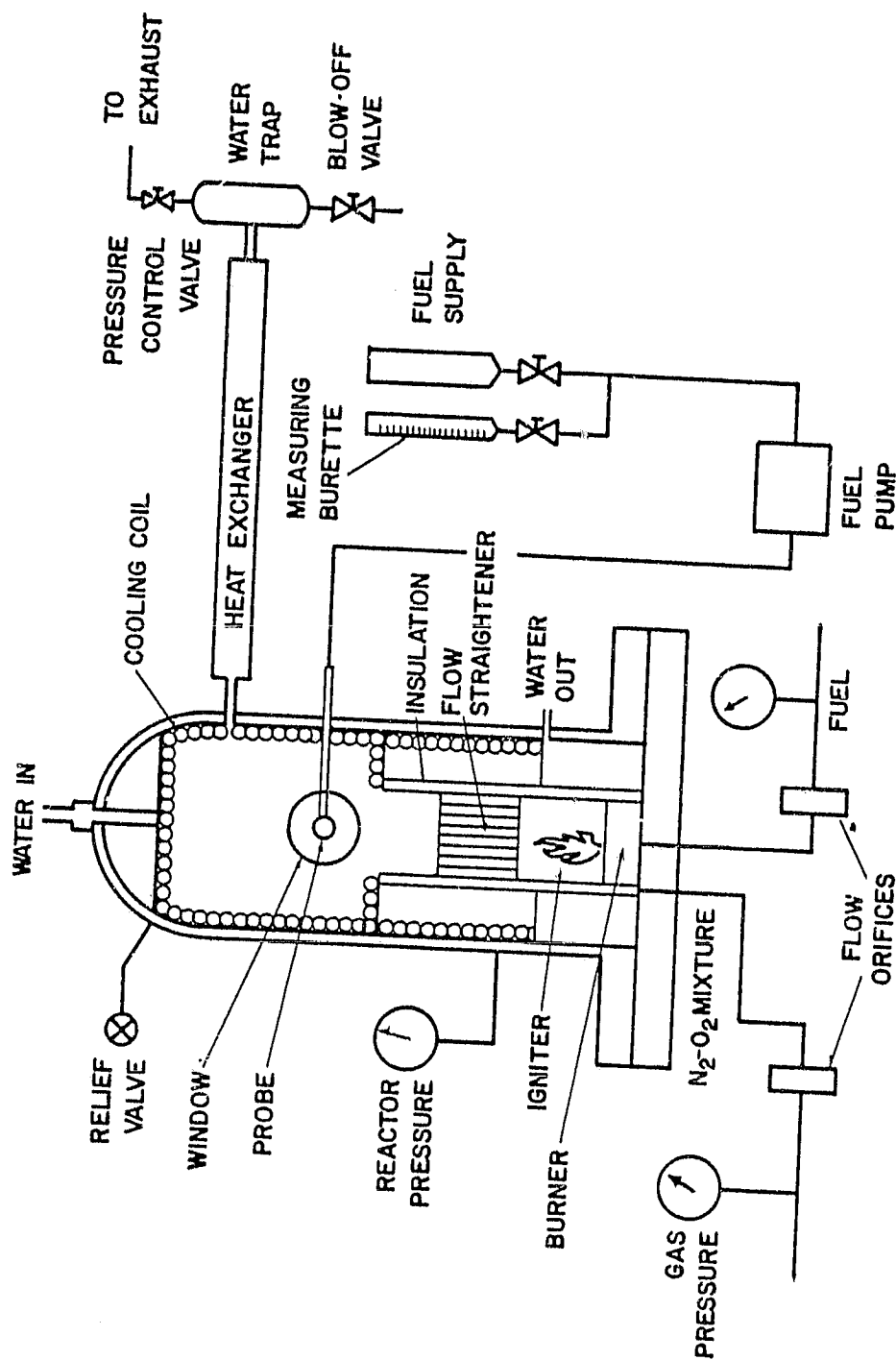


Fig. 7 Sketch of the high pressure burner apparatus.

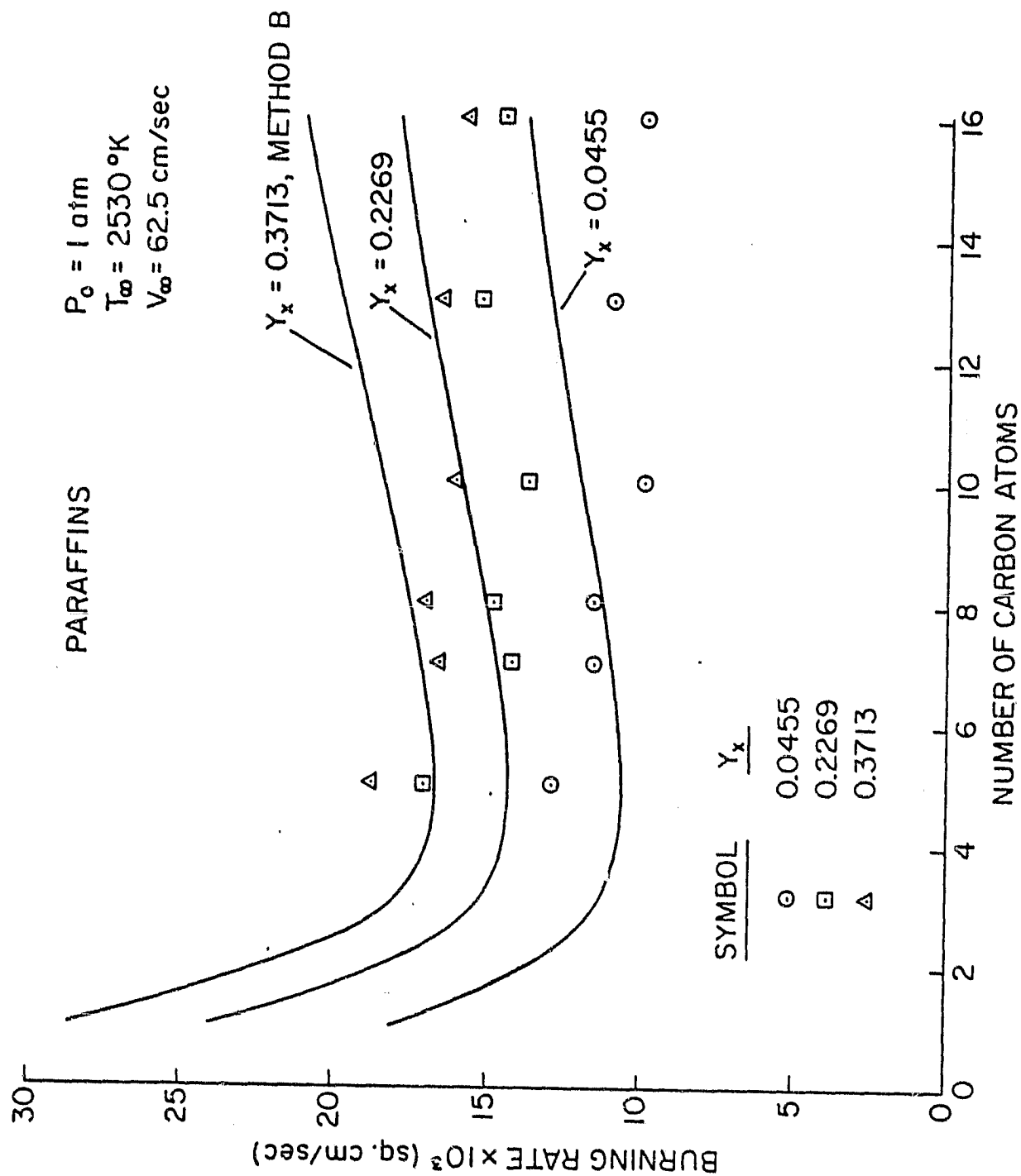


Fig. 8 Theoretical and experimental drop burning rates for various paraffins in a flowing combustion gas environment at atmospheric pressure: Gas velocity, 0.625 m/s; gas temperature, 2530 K; drop diameter, 1100 μm .

where K is called the burning rate constant. The burning rate constant is illustrated in Fig. 8 as a function of fuel type for various normal paraffins. Ambient oxygen concentration is a parameter on this plot. The temperature level of the tests is 2530 K. The convection correction for these conditions is less than 23 percent of the no-convection prediction (25).

There is fair agreement between theory and experiment in Fig. 8. The effect of oxident concentration is well represented. The effect of fuel type is somewhat less satisfactory. Other investigators have also observed that conventional drop burning theories tend to overestimate measurements for heavier hydrocarbons (58). This behavior is still not fully resolved, effects of variable properties and gas phase fuel decomposition have been suggested as possible reasons for the difficulty. Results for alcohols were similar to the findings for paraffin hydrocarbons. In general, the theory provides a reasonably sound means of estimating the effects of ambient composition, temperature and pressure on drop burning rates for a given fuel. Fuel type effects, however, are best handled by matching the prediction with measurements for at least one condition. There is sufficient uncertainty in physical properties for the gas phase, even for so-called variable property models, that a proper match can generally be achieved by adjusting properties within reasonable bounds.

Figure 9 is an illustration of measured fuel burning rates for porous spheres, burning in air, as a function of pressure. Various normal paraffins are considered, under natural convection conditions. Theoretical results are compared with the measurements, considering both the low and high pressure phase equilibrium theories. The theoretical curves are terminated at their high pressure end when the critical burning pressure is reached. The experimental results are terminated at high pressures due to problems with carbon spots forming on the surface of the sphere. Both theories are in reasonably good agreement with the measurements. The major difference between the theories is that the low pressure theory predicts a lower critical combustion condition, as noted earlier for drops.

Results for alcohol fuels were similar to the findings illustrated in Fig. 9. Since lower alcohols produce less soot, it was possible to observe supercritical combustion with methanol and ethanol at pressures in the range 80-100 atm. For supercritical combustion conditions, the fuel flow rate could be varied arbitrarily and no dripping of fuel was observed. Increasing the fuel flow rate simply caused the flame to move away from the surface. Similar effects are observed for the combustion of gases from porous spheres.

The effect of sphere diameter was examined for diameters in the range 6.4-19 mm. The theories accurately predicted the influence of diameter on the burning rate, under natural convection conditions. The effect of combustion gas environments was also considered. The results were similar to Fig. 9. In general, the discrepancy between

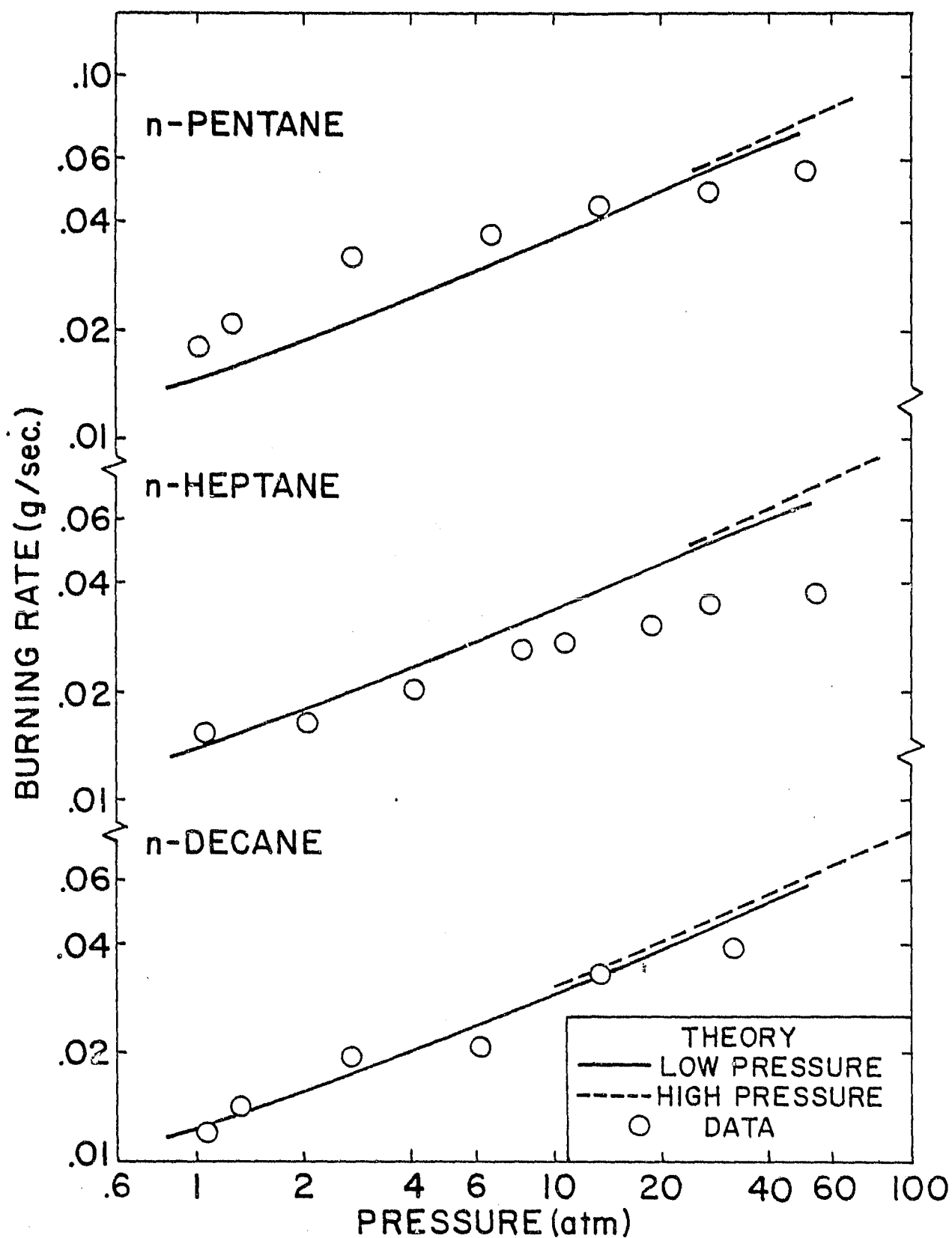


Fig. 9 Porous sphere burning rates of paraffins in air, for fuel inlet and ambient temperatures of 300 K. Sphere diameter, 9.5 mm.

theory and predictions was greatest when the ambient temperature was high and the ambient oxygen concentration was low.

Figure 10 is a comparison of the overall agreement between theory and experiment for combustion gas environments. The data includes both the baseline results at atmospheric pressure (25), and high pressure results (30). The convection correction was substantial for high pressure conditions. The data points shown on the figure correspond to the use of ambient properties in the convection correction, which was a procedure advocated by some investigators (25). Better agreement was obtained using average properties in this correction. The individual points when average properties are used are not shown on Fig. 10, in order to avoid cluttering the figure; however, the bounds of the data are indicated by the lines A-A. The choice of average or ambient conditions in the convection correction for the Faeth and Lazar (25) data is not very significant, since the correction was small for these test conditions. The test conditions for all the data illustrated in Fig. 10 are summarized in Table 2.

Figure 11 is an illustration of predicted liquid and gas phase compositions, at the liquid surface, for porous sphere combustion in a combustion gas environment. The gas phase composition remains relatively constant as the total pressure is increased. However, the liquid phase composition of dissolved gases increases steadily with increasing pressure. The thermodynamic critical point is indicated by the condition where the composition of both phases is the same. The results are similar for drop combustion, except that the highest pressure for subcritical combustion is not the mixture critical point, and the composition of both phases are not the same at this condition.

Conclusions. The low and high pressure theories yield roughly the same burning rate prediction. The major difference between these models is that the high pressure theory predicts a higher pressure for critical combustion. Predictions of critical combustion using the high pressure model are in reasonably good agreement with measurements. The use of constant or variable properties in the gas phase models had little impact on the results, as long as any constant property was selected at an arithmetic average condition. This is particularly important for convection corrections, where average properties should be used, c.f. Fig. 10. Following these prescriptions, burning rates for combustion gas environments could be predicted with an average error of 30%, over the range of variables summarized in Table 2. More accurate results can be obtained by matching theory and experiment for at least one operating condition, since existing theories are least effective concerning effects of fuel type.

Similar to the results discussed in Section 2.3.1, the high pressure model provided the best prediction of liquid surface temperatures. Dissolved gas concentrations become very significant at high pressures, e.g., reaching values approaching 50 percent in Fig. 11. This tends to

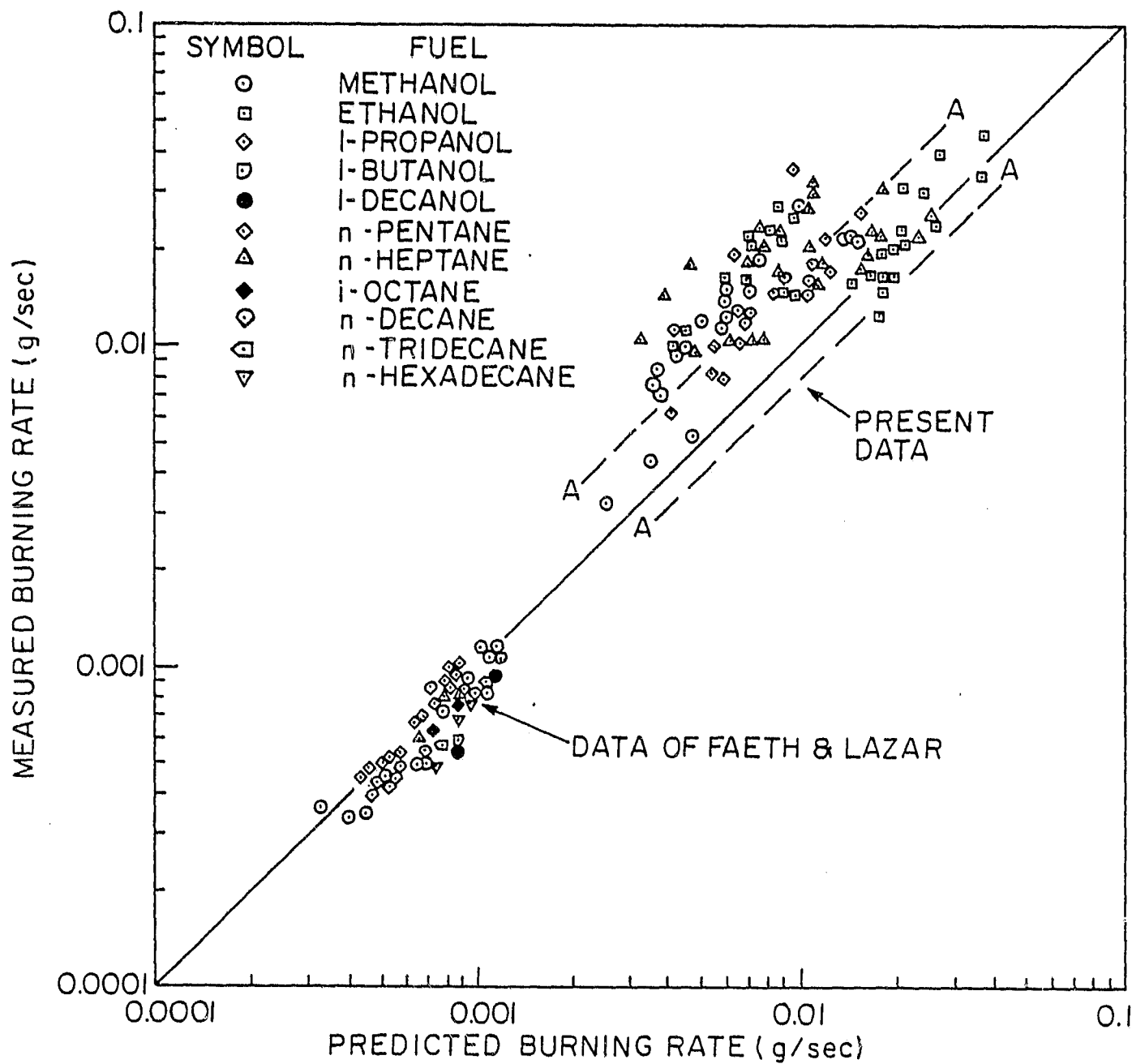


Fig. 10 Overall comparison of theoretical and experimental gasification rates in combustion gas environments. Lines A-A are data bounds when average properties are used in the convection correction.

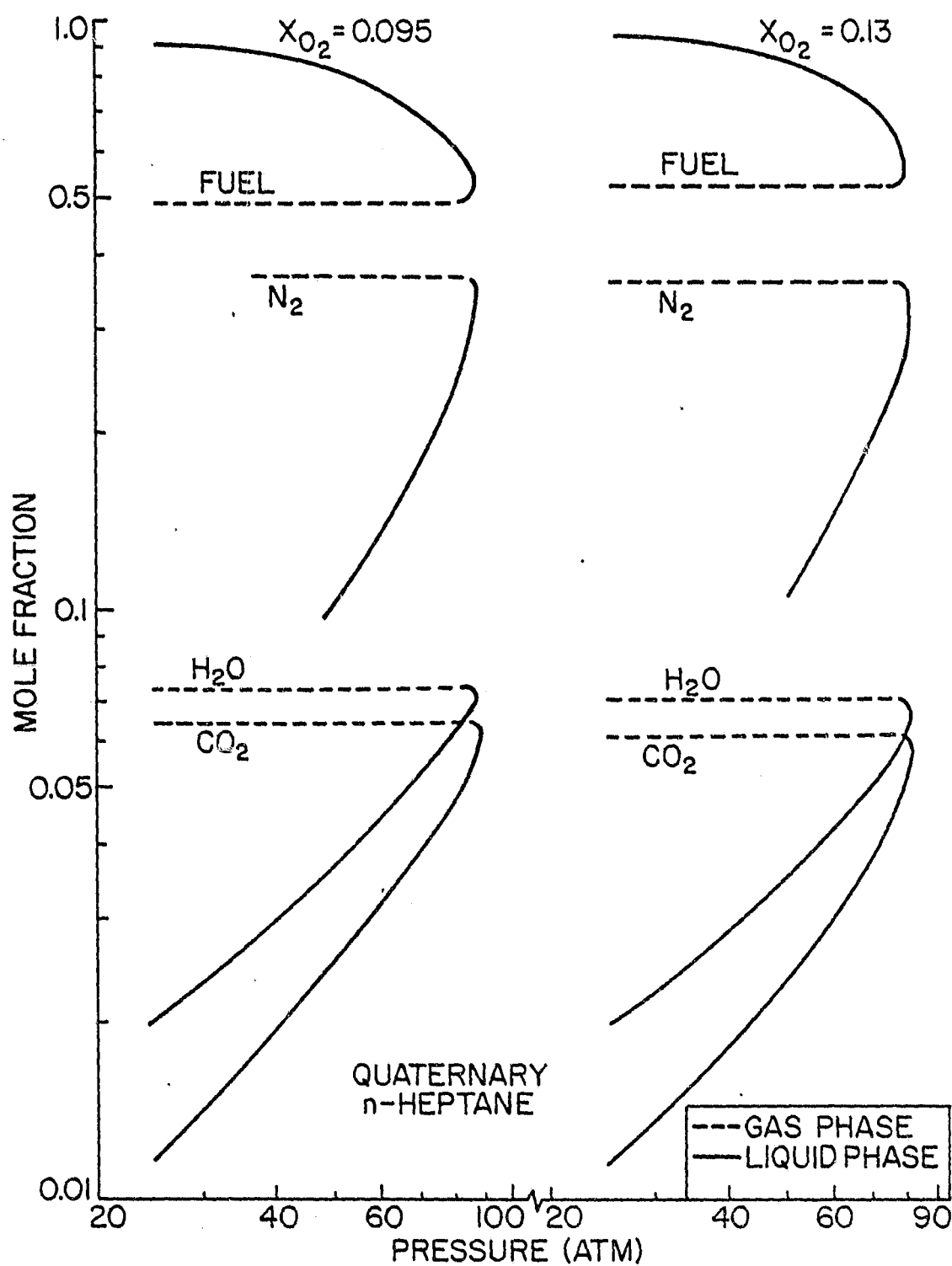


Fig. 11 Predicted liquid-surface compositions for porous sphere combustion. Ambient temperature 1145 K, Fuel inlet temperature 300 K.

Table 2

Summary of Test Conditions for Drop Combustion
Rates in Combustion Gas Environments

	Canada and Faeth (30)	Faeth and Lazar (25)
Test Method	Porous Sphere	Suspended Drop
Ambient Temperature (K)	600-1500	1660-2530
Ambient Oxygen Conc. (mole %)	0-13.5	0-41.8
Pressure (atm)	1-40	1
Diameter (μm)	9500	1100
Reynolds number (approach properties)	40-680	1.3-2.2

raise the critical pressure of the mixture at the liquid surface, and reduce the critical temperature, from that of most hydrocarbon fuels. The net result is that critical combustion occurs at pressures in excess of the critical pressure of the pure fuel.

III. COMBUSTION OF HYDRAZINE FUELS

3.1 Introduction

Hydrazine and its derivatives, MMH (monomethylhydrazine) and UDMH (unsymmetrical dimethylhydrazine) are capable of exothermic decomposition, and can be used as monopropellants as well as the fuel component of a bipropellant system. In either case, fuel decomposition occurs in the gas phase near the liquid surface, which can greatly increase the drop gasification rate in comparison to conventional bi-propellants. When burned in an oxidizing atmosphere, the decomposition flame near the surface can be surrounded by an oxidization zone, yielding a hybrid structure. Existing information on the combustion mechanism of hydrazine fuels was relatively limited, in view of the complexities of the decomposition process and the possibility of hybrid flame structures (59-63). Therefore, some of the experimental techniques developed during the high pressure bipropellant drop combustion study were applied to the hydrazine fuels.

A second area of interest for hydrazine fuels involves the problem of combustion instability. Gasification rates for monopropellant drops vary more rapidly with pressure than is the case for conventional bi-propellants. This suggests a greater tendency for combustion instability with these fuels (see Ref. 64 and references cited therein).

Both the problem of steady combustion and the combustion response of drops and sprays of hydrazine fuels were considered during the investigation.

3.2 Steady Drop Combustion

Introduction. Earlier work on hydrazine combustion (59-63) was extended by burning hydrazine, MMH and UDMH droplets in a combustion gas environment. The test environment included ambient oxygen concentrations in the range 0-42% by mass, and ambient gas temperatures of 1660-2530 K, at atmospheric pressure. Both supported drops and porous spheres were employed in the tests, in order to obtain a relatively large drop diameter range, 1.1-19.1 mm.

A simplified theoretical model of hybrid combustion was developed, employing an approach suggested by Williams (64).

Further details concerning this portion of the investigation can be found in Refs. 7, 8, 26, 27 and 42.

Apparatus. The experiments employed the flat flame burner apparatus, illustrated in Fig. 6. For suspended droplet tests, the drops were mounted on a 100 μm diameter quartz fiber. The arrangement of the porous sphere tests was similar to that pictured in Fig. 7.

Shadowgraph motion pictures were analyzed to provide the drop diameter variation as a function of time for the suspended drop tests. This information allows the drop burning rate to be computed (26). The fuel flow rate to the sphere, with the sphere fully wet and not dripping, provides the burning rate directly, for the porous sphere tests.

Theory. The objective of the theoretical model was to provide a semi-empirical correlation of the burning rate data. The model considers the presence of both a decomposition and an oxidation flame. Each reaction zone is assumed to be infinitely thin. The position of the decomposition flame is fixed by its laminar flame speed, which is correlated empirically. The position of the oxidation flame is fixed by diffusion rates and the requirements of stoichiometry. Convection effects are considered using a film theory approximation. The same empirical correlation for convection used for the bipropellant combustion theory was employed to compute the film thickness. The low pressure phase equilibrium model is adequate for the test conditions and was employed in the analysis.

The theory provides predictions of the position of the two flames, the droplet gasification rates, the temperature of the liquid surface and both flame temperatures.

Results and Discussion. The burning rate of hydrazine as a function of drop diameter is illustrated in Fig. 12 for a typical oxidation condition. Burning rate estimations from both the hybrid combustion model and the conventional bipropellant model, which neglects the presence of the decomposition flame, are also shown on the figure. The bipropellant results are shown as a band rather than a single curve, in order to illustrate the effect of property uncertainties. The hybrid model contains the activation energy, E , as a parameter in the laminar flame speed correlation. This parameter has little influence on the results over most of the data range illustrated in Fig. 12. The hybrid model clearly provides better agreement with the measurements. The effect of reaction is illustrated by the relatively rapid increase in drop burning rate with size. At smaller sizes, however, the decomposition flame tends to merge with the oxidation flame, and the two predictions are essentially the same. Similar results were obtained for various ambient oxygen concentrations, temperatures and fuels (25).

Figure 13 is an illustration of the comparison between all the predictions and measurements for hydrazine. In addition to the results of the present investigation, data from Refs. 59-62 are also considered. The average error between predictions and measurements is 20 percent. Comparisons for MMH and UDMH yielded similar average errors. The data range for the comparison is summarized in Table 3.

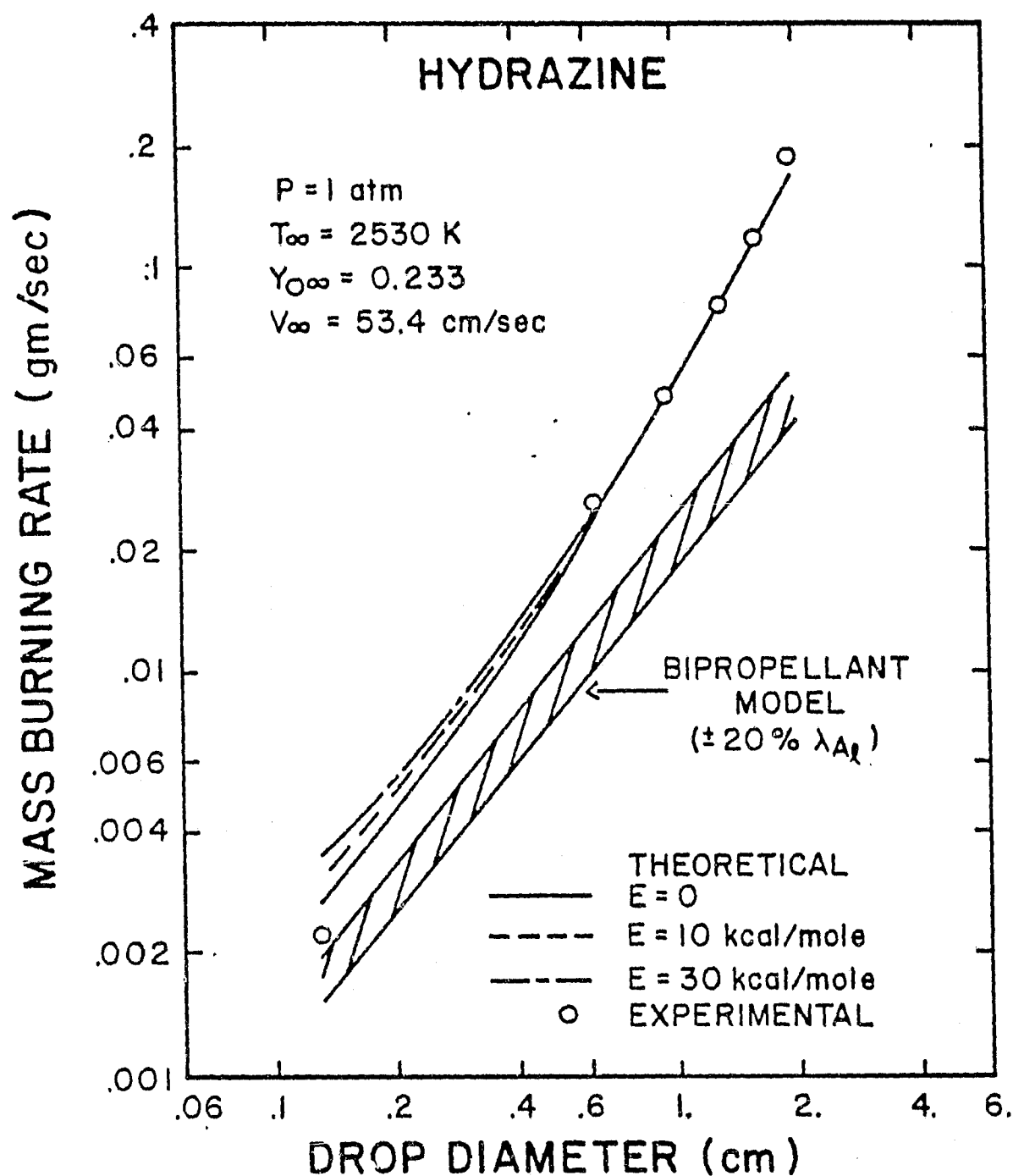


Fig. 12 Hydrazine burning rate as a function of drop diameter for a typical oxidation condition.

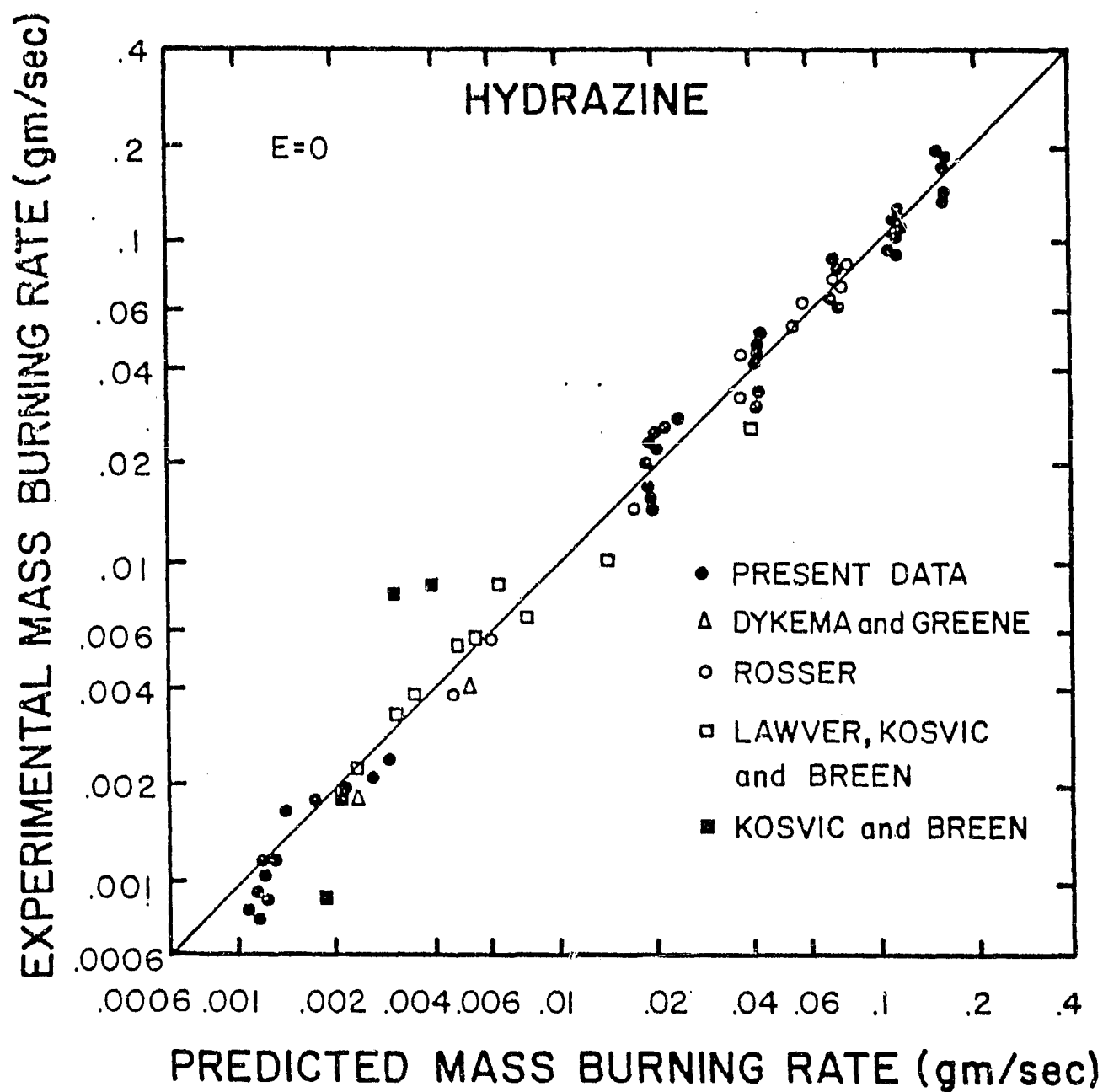


Fig. 13 Comparison of predicted and measured burning rates for hydrazine.

Table 3

Summary of Test Conditions for Drop Combustion Rates
of Hydrazine Fuels

Fuels	Hydrazine, MMH, UDMH
Drop diameters	0.38 - 19.1 mm
Ambient temperature	300-2530 K
Ambient oxygen concentration	0-100%
Pressure	1-7.8 atm

Conclusions. Although a more rigorous theory would be desirable, the comparison between the hybrid combustion theory and the experiments was satisfactory, with average errors less than 20%. Hydrazine, UDMH and MMH all exhibited hybrid combustion effects at atmospheric pressure, although the effect was most pronounced for hydrazine. The influence of pressure has not been clearly resolved during this investigation, although a second-order dependence for the laminar flame speed of hydrazine is suggested by the measurements of Kosvic and Breen (62), at least at pressures up to 7.8 atm. Results discussed in the next section confirm the second-order dependence at pressures greater than atmospheric pressure.

3.3 Combustion Response of Liquid Hydrazine Fuels

3.3.1 Liquid Strand Combustion

Introduction. In response to combustion instability problems in liquid fueled rocket engines, several studies have been completed concerning the open-loop combustion response of bipropellant droplets (63). The present investigation considered this problem for monopropellants.

The investigation was limited to the open-loop response to pressure fluctuations, since earlier work had shown that response to velocity fluctuations was small (63). The regime that was treated does not involve the low frequency range where both liquid- and gas-phase processes are quasisteady. The results are limited to conditions where transient liquid and gas-phase phenomena, or thermal waves, are interacting with the combustion process. The limiting case of a constant area liquid strand was considered in the first phase of the study. This portion of the study is discussed in this section. Strand combustion is representative of very large droplets, with the reaction zone close to the surface, where curvature effects are small. The response of smaller drop sizes and sprays is discussed in Section 3.3.2.

The predictions were verified directly by experiment - apparently the only case where this has been done for a liquid combustion response problem. Hydrazine was used as the test fuel, since it can sustain combustion at very low burning rates. With such a material, interactions between the combustion process and the transient liquid thermal wave, due to pressure fluctuations, can be observed at modest frequencies, simplifying the measurements.

Complete details concerning this portion of the investigation can be found in Refs. 10, 12, 29 and 43.

Apparatus. A sketch of the apparatus used to measure the open-loop response of liquid hydrazine strands appears in Fig. 14. The liquid was contained in a glass tube and ignited at the top with an electrically heated wire. Combustion caused the liquid surface to move down the tube, past the observation windows.

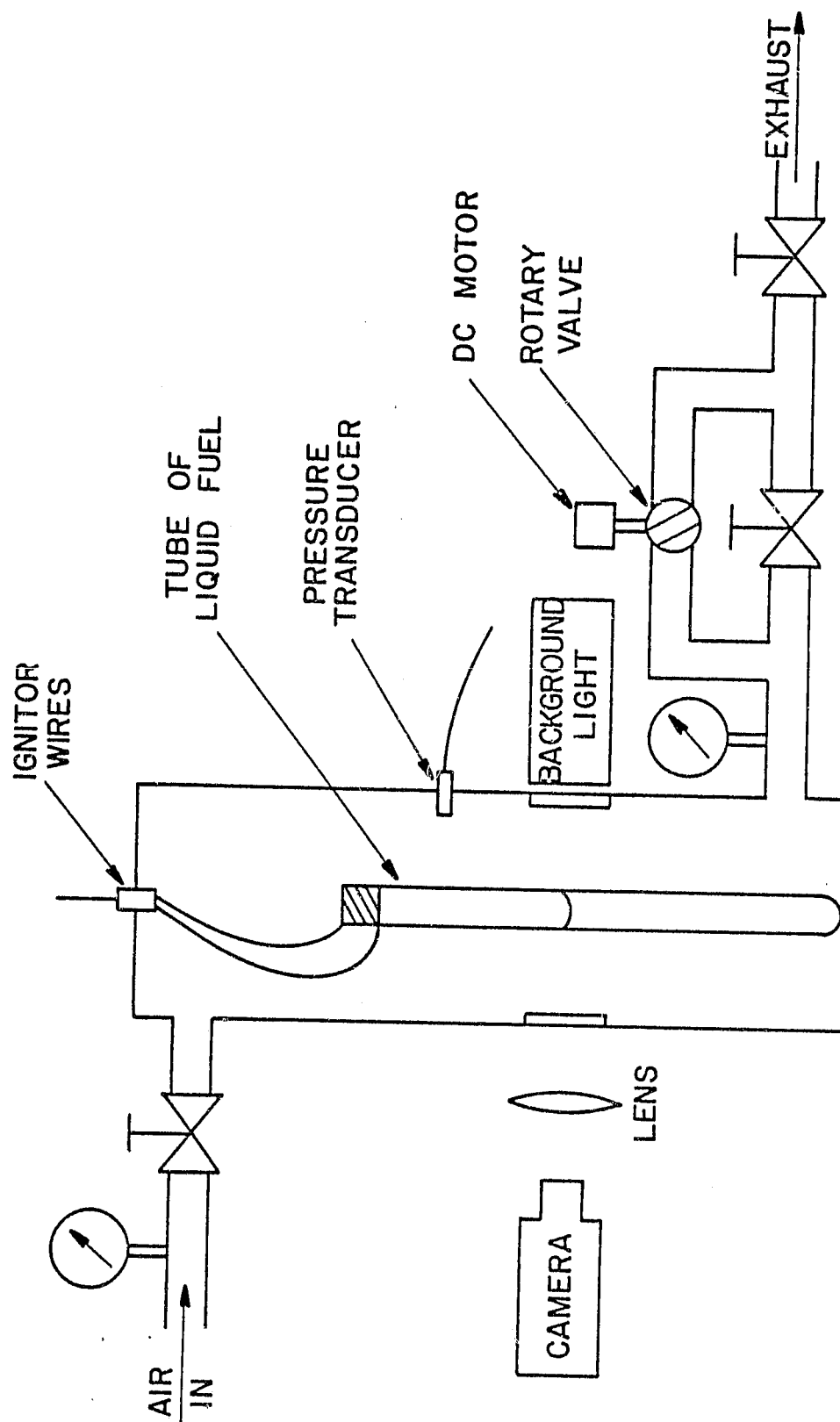


Fig. 14 Sketch of the oscillatory strand combustion apparatus.

A rotary valve arrangement was used to provide oscillatory pressure variations within the test chamber. This system allowed independent variation of the mean pressure, and the amplitude and frequency of the pressure oscillations.

The motion of the liquid surface was recorded as a shadowgraph on a 35 mm strip camera. The overall optical gain of the surface position measurements was 125.1.

Theory. The analysis for the open-loop response of a liquid mono-propellant was similar to the solid-propellant combustion analysis of Tien (65). The model considers both gas- and liquid-phase transient effects, and variable properties are treated in the gas phase. The combustion process is assumed to be one-dimensional, premixed, and laminar, following a one-step, irreversible chemical reaction. In the gas phase, the molecular weights of all species are taken to be constant and equal, the gas is ideal, the Lewis number is unity, and the thermal conductivity is assumed to be independent of composition and proportional to temperature. The liquid phase properties are assumed to be constant, with negligible reaction and dissolved gas concentrations. Low pressure phase equilibrium is assumed at the liquid surface.

A perturbation analysis is used to complete the solution. Terms up to first-order were considered. The zero-order results were checked with steady combustion results, prior to treating combustion response with the first-order theory.

Results and Discussion. The predicted and measured steady burning rates of hydrazine as a function of pressure are illustrated in Fig. 15. Data from both the present study and Antoine (66) are shown. The two sets of measurements are in reasonably good agreement. The present measurements are properly corrected for flame curvature, due to surface tension, and probably are more accurate than the results of Ref. 66.

The theoretical results illustrated in Fig. 15 were obtained by fitting the zero-order (steady) theory at a particular condition, for various reaction orders and activation energies. Subsequent results are predictions. The effect of activation energy on the correlation between predictions and measurements is small. The reaction, however, shifts from first to second order at pressures near 2 atm and two separate correlations are needed to cover the range of the data. Predictions of liquid surface temperatures and the temperature distribution in the liquid phase were also examined. Agreement between theory and experiment was excellent (31,43).

Having obtained a reasonably satisfactory model for steady combustion, oscillatory combustion was considered. Since the theory is linear, the effect of the amplitude of the pressure oscillation was examined. It was found that the amplitude of the burning rate oscillation was linear for pressure oscillations less than 20 percent of the mean pressure. Subsequent tests were limited to pressure amplitudes less than 15 percent of the mean pressure, in order to assure operation in the linear range for comparison with the linear response theory.

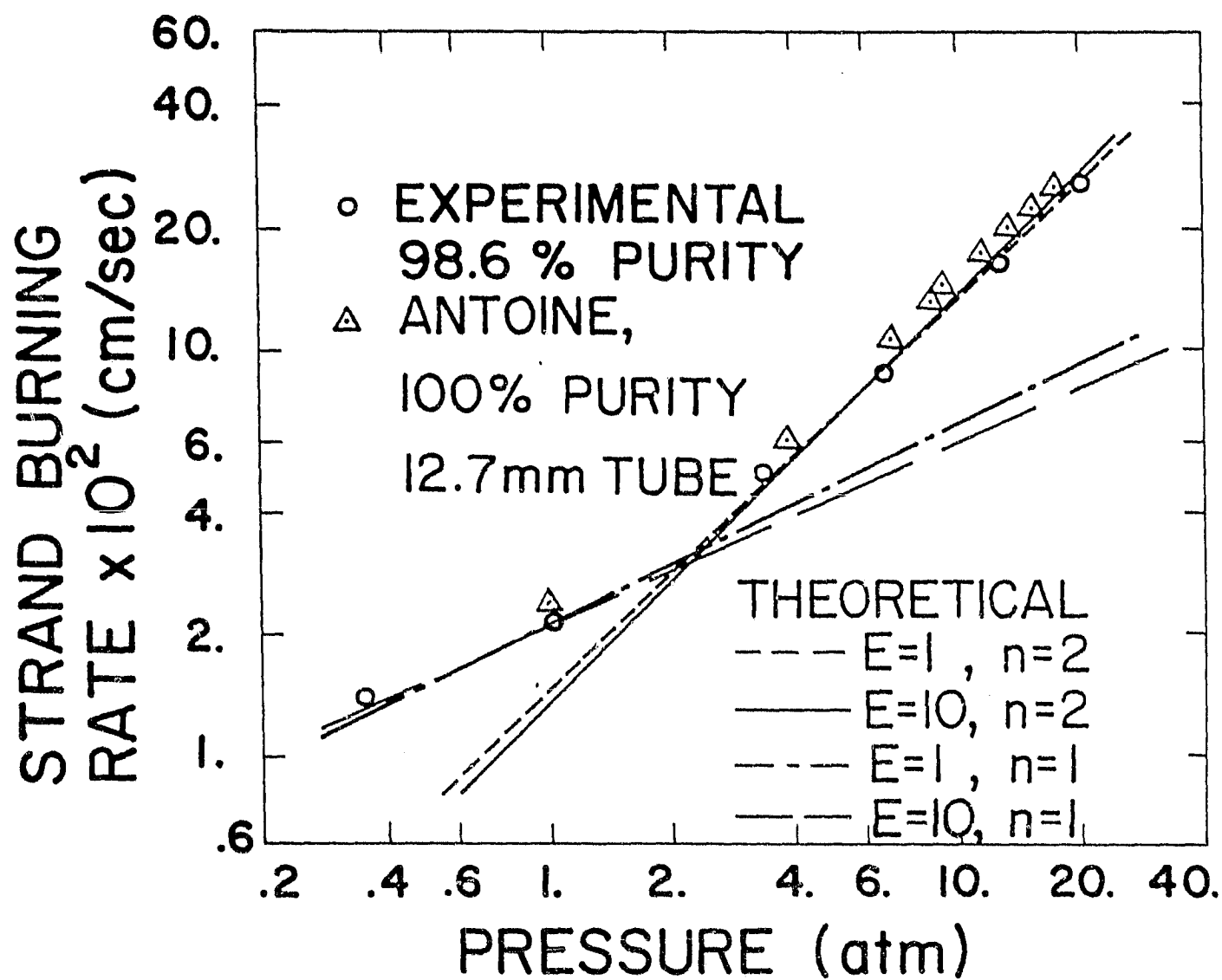


Fig. 15 Theoretical and experimental steady hydrazine strand burning rates as a function of pressure.

Figures 16 and 17 are illustrations of the comparison between predicted and measured amplitudes and phase angles of the liquid surface oscillations as a result of imposed pressure oscillations of a given frequency. Theoretical results are illustrated for various activation energies. A second-order reaction is assumed for the mean pressure of these results, 9.77 atm, c.f. Fig. 15. The best match between theory and experiment is obtained for a dimensionless activation energy in the range 10-15.

Employing the chemical parameters determined from the experiments, the real part of the acoustic admittance was computed for hydrazine strand combustion. A typical result is illustrated in Fig. 18. As the imposed frequency is increased, two positive admittance peaks are observed. The first peak is due to the interaction between the combustion process and liquid phase transient effects while the second peak is due to gas phase transient processes. These characteristics are similar to T'ien's (65) results for solid propellants. Increasing the pressure tends to increase the magnitude of the first peak and decrease the magnitude of the second peak.

Combustion instability is usually associated with values of the real part of the acoustic admittance greater than a value on the order of unity. At atmospheric pressure, only the gas phase transient range has sufficient amplification to drive instability. At pressures greater than 10 atm, however, both regimes are significant. Table 4 is a summary of the actual frequency ranges where the acoustic admittance exceeds unity. Combustion instability is usually associated with frequencies in the range 500-30,000 Hz (63). At pressures greater than 10 atm, the ranges shown in Table 4 suggest that the liquid phase mode is the dominant regime in this frequency range.

Conclusions. The combustion mechanism of hydrazine shifts from first to second-order at pressures slightly greater than atmospheric pressure. Linear combustion response was observed directly, the only case where this has been done for liquids. Theory and experiment were in good agreement with respect to both mean properties and combustion response. The analysis correctly predicted a complex variation of the phase shift with pressure. Both liquid and gas phase transient effects interact with the combustion process to produce frequency ranges when the acoustic admittance exceeds unity. However, liquid transient phenomena appear to be more important for the stability of typical combustion systems at pressures greater than 10 atm. These results are limited to burning liquid hydrazine strands, which are only representative of the largest drops in actual combustion chambers.

3.3.2 Drop and Spray Combustion

Introduction. Large monopropellant drops behave similar to burning liquid strands, and would show positive combustion response regions similar to the results discussed in Section 3.3.1. On the other hand, reaction effects become small for small drops, suggesting

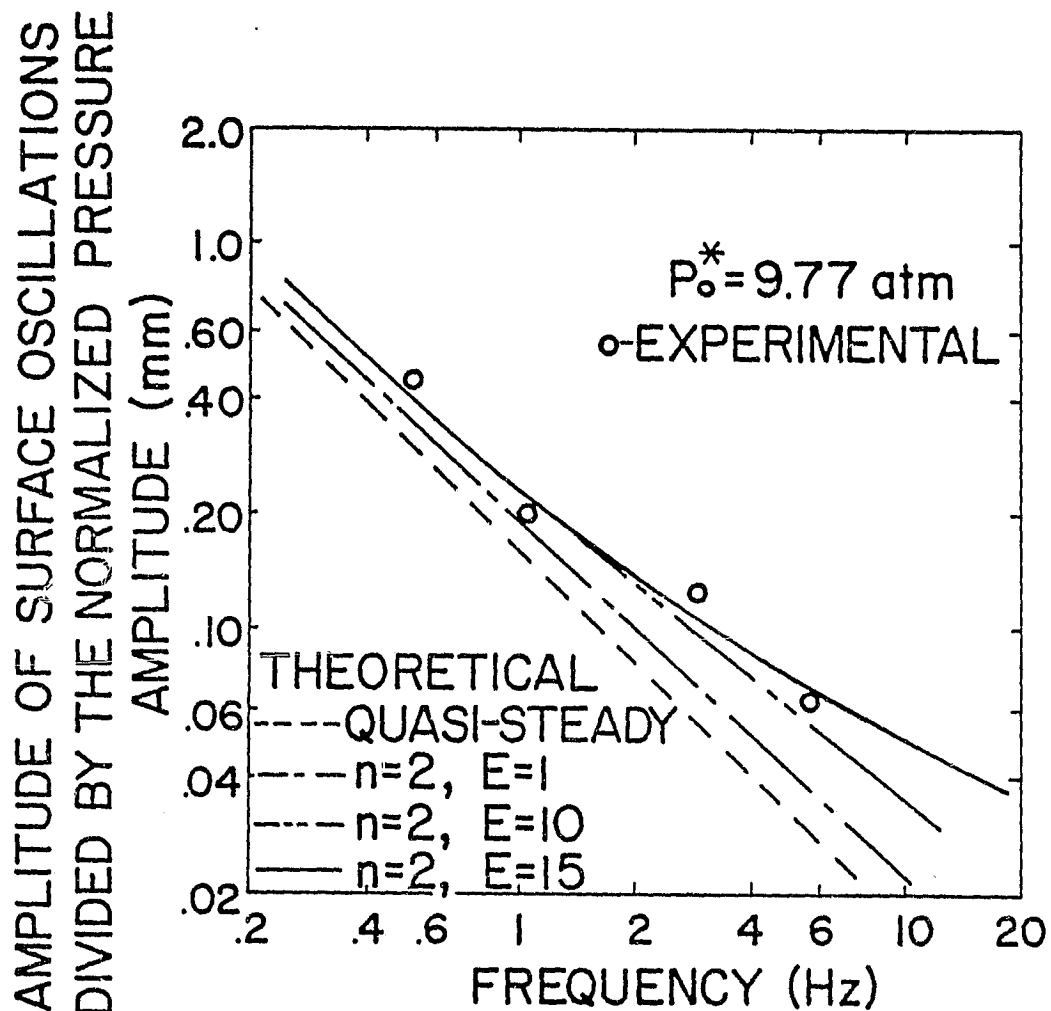


Fig. 16 Theoretical and experimental magnitude of the liquid surface oscillation of burning hydrazine as a function of the frequency of the imposed pressure oscillation.

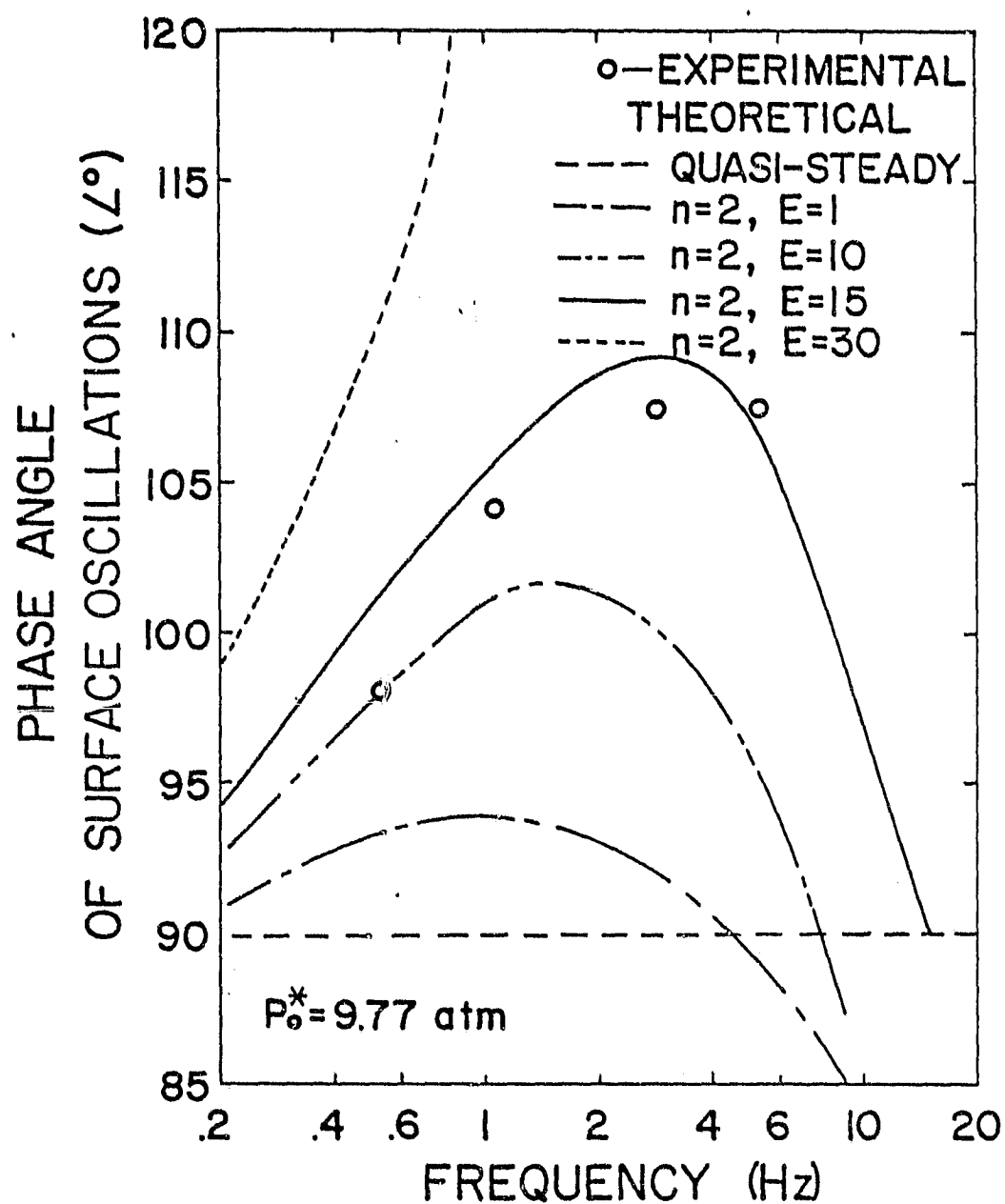


Fig. 17 Theoretical and experimental phase angle of the liquid surface oscillation of burning hydrazine as a function of the frequency of the imposed pressure oscillation.

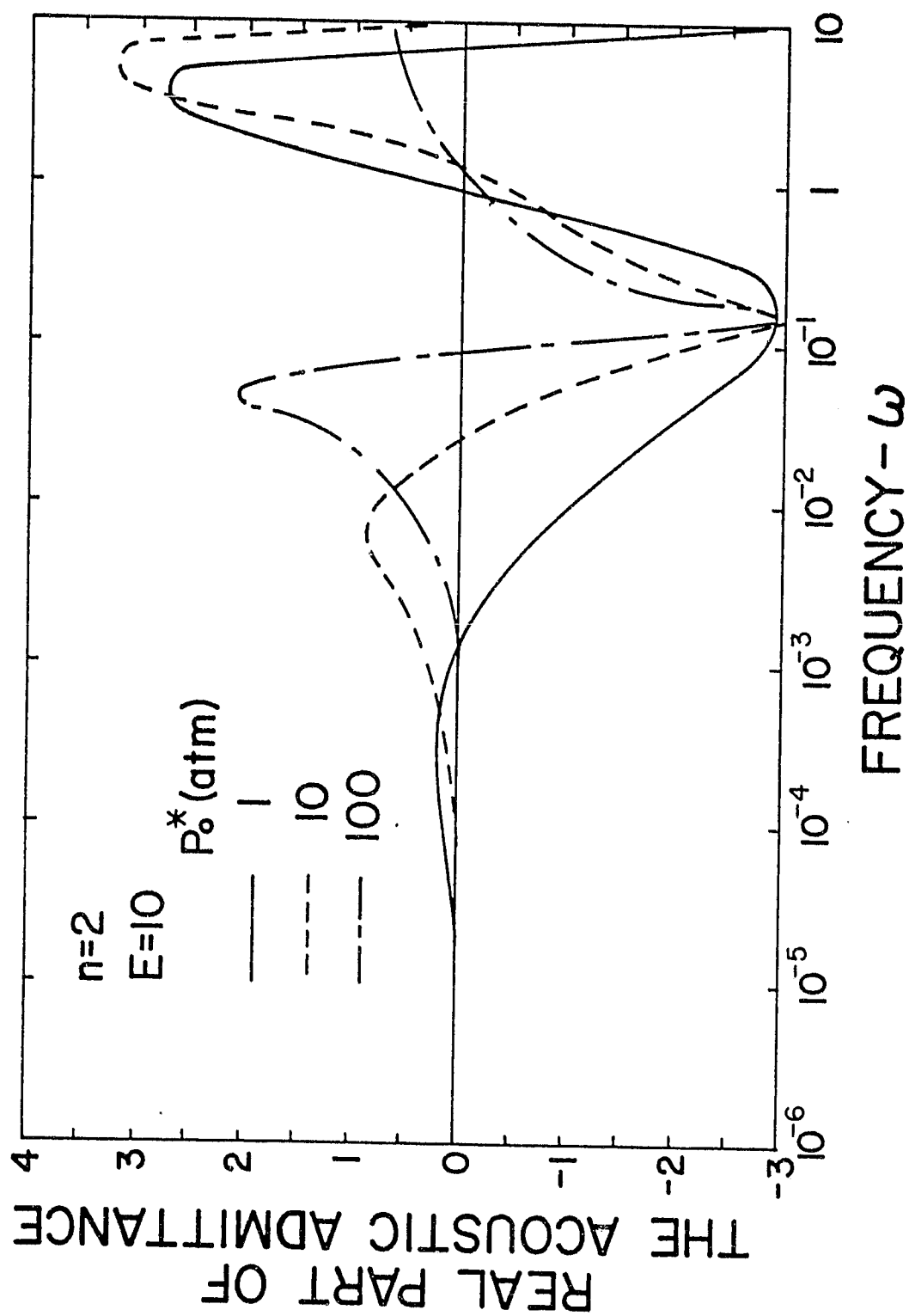


Fig. 18 Predicted real-part of the acoustic admittance for hydrazine strand combustion.

Table 4Frequency Ranges for Potentially Unstable
Combustion of Hydrazine

Mean Pressure (atm)	Liquid Transient Range (Hz)	Gas Transient Range (Hz)
1	-	300-1500
10	15 (approx)	4500-21500
100	450-1650	>225,000

that their response characteristics would be similar to conventional bipropellant drops. Earlier results indicated that the response of bipropellant drops, by interaction of combustion with liquid and gas phase transient effects, was small (63). The objective of the present investigation was to examine the transition between these two regimes and to also make a preliminary assessment of spray response.

The study was limited to hydrazine combustion. The theory was largely based on the earlier results for hydrazine strand burning response. As noted earlier, the response under consideration is not that of a combustion chamber as a whole, where both liquid and gas phases are quasisteady. Emphasis was placed on the interaction between the combustion process and the transient thermal wave in the liquid phase, in the presence of imposed pressure oscillations.

Further details on this portion of the study may be found in Refs. 14, 15, 32, 33 and 45.

Theory. Most of the basic elements of the model were the same as for the strand combustion case. The model considers gas-and liquid-transient effects. Variable physical properties are treated in the gas phase. To simplify the analysis, forced convection was neglected, providing a spherically symmetric combustion process. This limitation is less serious for monopropellants than bipropellants. The response is greatest where the reaction zone is near the liquid surface, a condition where the combustion process is not strongly affected by forced convection (67,68).

The ambient pressure is assumed to be oscillating with a wavelength that is long in comparison to the dimensions of the drop combustion field. The period of oscillation, however, is assumed to be short in comparison to the drop lifetime. This assumption applies a low frequency bound for the analysis. Low pressure phase equilibrium was assumed at the liquid surface.

A common assumption for drop combustion studies is that the drop is heated uniformly to its wet-bulb temperature. It is generally recognized, however, that temperature gradients persist within drops throughout their lifetime, as artifacts of the heat-up period. The high mean combustion rate of monopropellants increases the possibility of temperature gradients (69). In order to investigate the potential affect of temperature gradients on combustion response, two limiting cases were treated: i) mean liquid temperature varying as though a quasisteady combustion wave was propagating toward the center of an unheated drop, and ii) mean liquid temperature constant at the wet-bulb temperature.

Similar to the strand analysis, a perturbation solution was employed. The zero-order solution provides the steady combustion characteristics. The first-order solution provides the linear combustion response.

Analysis was also completed to determine the response of a spray, given the response of individual drops. This response was defined in terms of the mass burning rate fluctuation, averaged over the particular drop size distribution in the spray, normalized by the total steady burning rate of the spray.

Results and Discussion. Figure 19 is an illustration of droplet response as a function of frequency and drop size (the parameter A is proportional to drop diameter squared), for non-wet-bulb combustion. The gas phase is assumed to be quasisteady for these results. The response generally increases as A , or the drop size, increases. For non-wet-bulb combustion, a response peak is observed at frequencies near the characteristic frequency for liquid phase transient effects (this is not observed for wet-bulb combustion). For large values of A , the system approaches the characteristics of strand combustion. In this range, the response is unity at low frequencies, where both phases are quasisteady. This occurs since the burning rate is proportional to pressure for steady strand combustion with a second-order reaction. Droplets evaporating with little reaction near the surface (low values of A) generally exhibit low or negative response for all frequencies, in agreement with earlier studies for bipropellant drop response.

Figure 20 is an illustration of spray response calculations for non-wet-bulb combustion. Several spray distributions are considered involving initial injection of varying proportions of different drop size groups (ranging from 100 percent large drops to 100 percent small drops). The total response approaches unity when the two largest sized drops comprise only about 10 percent of the injected mass, corresponding to 0.3 percent of the drop injection rate. This indicates that even a very small percentage of large drops in a spray can result in substantial positive response. This occurs since the large drops comprise an appreciable fraction of the drops within a combustion chamber, due to their long lifetime, e.g., when the two largest groups comprise only 11 percent of the injected spray mass, drops originating from these groups provide 90 percent of the mass of fuel within the burning spray.

Conclusions. The response of monopropellant drops and sprays can exceed unity for drop sizes and frequencies representative of high-frequency combustion instability, providing a viable mechanism for this phenomena. In contrast, drop response for bipropellants yields low response values. The response is greatest for large drops, having mean liquid temperature gradients, at high pressures. Response factors were less than unity for drops at their wet-bulb state. The response of a monodisperse spray is less than the response of the injected drop-size, due to the reduced response of small drops. Response depends very strongly on the initial drop size distribution for polydisperse sprays; however, even a small percentage of large drops can provide appreciable response due to their long lifetimes and large response.

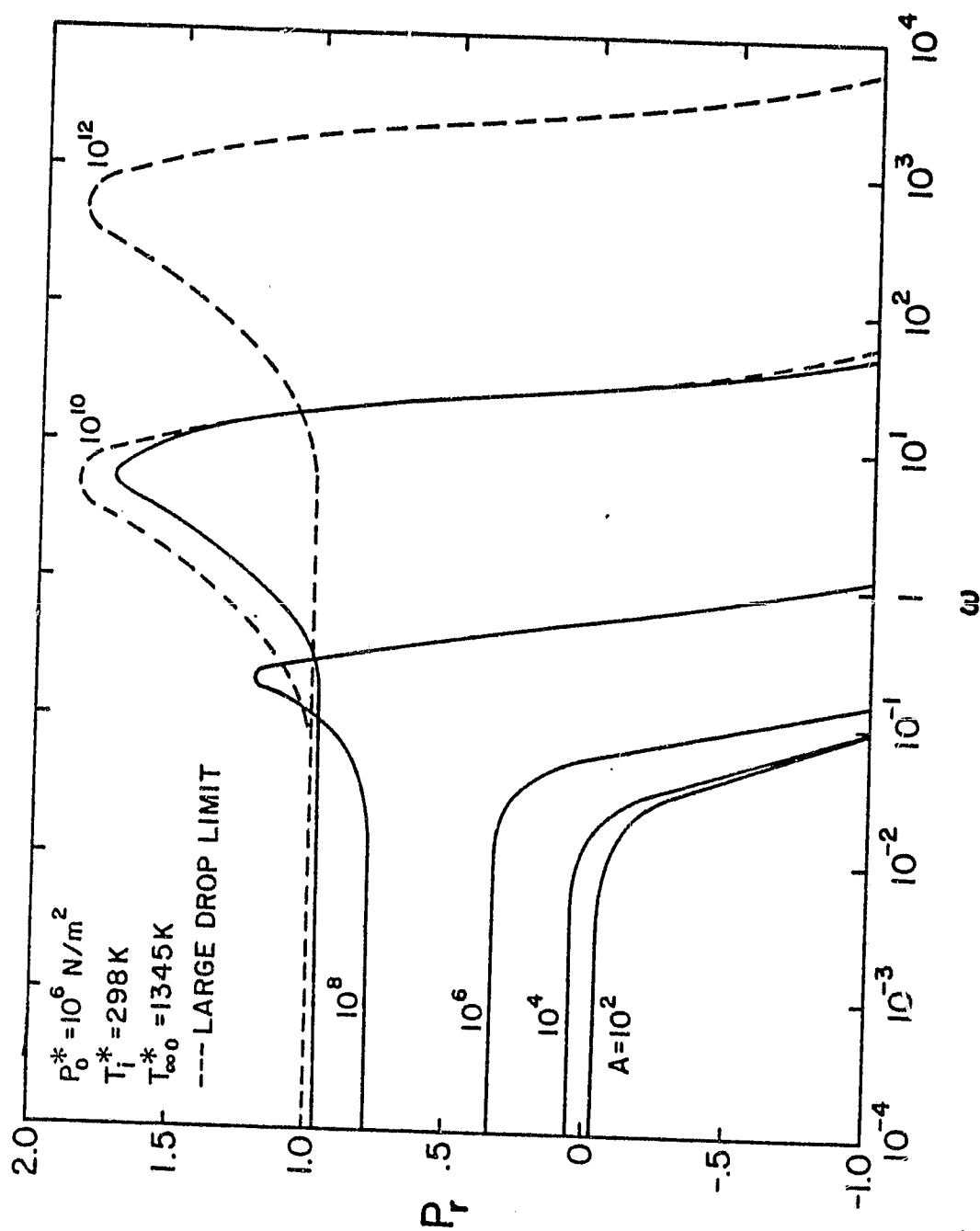


Fig. 19 Predicted hydrazine droplet response as a function of frequency and size.

$A_0(X10^8)$	% MASS IN CHAMBER			% DROPS/SEC. INJECTED			% MASS/SEC. INJECTED		
	123	10	.0123	123	10	.0123	123	10	.0123
————	100 ^a	0	0	100 ^a	0	0	100 ^a	0	0
-----	10	30	60	.001	.053	99.946	.1	1.4	98.5
-----	60	30	10	.005	.315	99.68	3.4	7.7	88.9
-----	49.5	49.5	1.0	.05	4.98	94.97	11.47	51.78	36.75
-----	0	0	100 ^a	0	0	100 ^a	0	0	100 ^a

^a ALL DROPS IN THE SPRAY ARE AT A
CONSTANT SIZE A_0

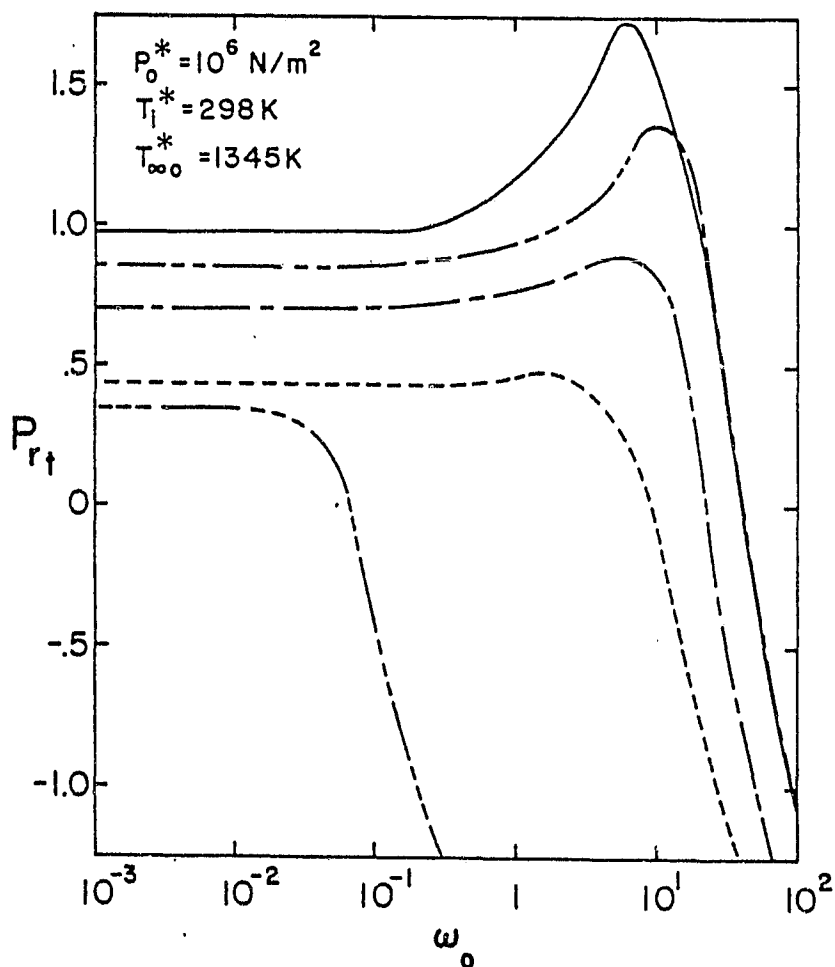


Fig. 20 Predicted response of a polydisperse hydrazine spray as a function of frequency.

IV. COMBUSTION OF SPRAYS

4.1 Introduction. The development of turbulence models with second-order closure, and the availability of general-purpose computer programs to solve complex systems of flow and combustion equations, has provided the potential to develop spray combustion models to assist combustor development efforts. In fact, models along these lines are already being used by some gas turbine manufacturers (36). A difficulty encountered with spray models, however, is the absence of data concerning spray characteristics produced by a given injector (injected drop size and velocity distributions for hot-firing conditions).

A long term objective of spray combustion studies is to develop comprehensive models where all factors can be predicted, including injector characteristics. There are many difficulties to be resolved, however, and simplified models can still provide useful results in the interim. One simplification that can be made, involves the assumption of locally homogeneous flow (LHF). This approximation implies that there is no velocity difference between the phases (no slip) and that the phases are in thermodynamic equilibrium, i.e., that the temperature and fugacity of all components is the same in all phases. This approximation is most appropriate for finely atomized sprays, where individual drops can rapidly respond to changes in their local environment, i.e., cases where the process is mixing controlled as opposed to being vaporization controlled. All real sprays exhibit some degree of slip and loss of thermodynamic equilibrium. In this case, the results of LHF, if accurate, represent an upper bound to the rate of development of the combustion process - the actual spray will develop more slowly.

Locally homogeneous flow models are widely used in the analysis of two-phase heat transfer and hydraulic problems (70). Models of this type have also been employed for gas-liquid jets with success, since bubbles respond rapidly to surrounding liquid flows (71,72). There has also been earlier application of the method to sprays. Onuma and Ogasawara (73) demonstrate startling similarities between measured properties in gas flames and well atomized sprays. Newman and Bruzustowski (74) also successfully apply the concept to sprays evaporating near their thermodynamic critical point. Models along these lines have also been successfully applied to Diesel combustion (36). On the other hand, Khalil and Whitelaw (75) evaluated a gas simulant model (this is not a complete locally homogeneous flow model, only the energy release, momentum and stoichiometry is matched, not the complete equation of state as in traditional locally homogeneous flow models) with less success, finding significant discrepancies between predictions and measurements for sprays having a Sauter mean diameter as small as 45 μm . Thus, adequate criteria for the validity of LHF models had not been determined in earlier work.

The present investigation extends this work, attempting to provide a more systematic evaluation of the LHF model. A systematic method of estimating the conditions where LHF models are accurate was also sought. The study was limited to a finely atomized spray, injected into a stagnant environment, in order to simplify the flow field. The theory employs a $k-\epsilon$ -g turbulence model, similar to those used for gaseous diffusion flames (76). This model has the advantage of minimizing the number of empirical parameters to be specified.

Since turbulence models contain a large number of empirical parameters, the evaluation proceeded through a series of simpler flows before sprays were considered. The sequence was as follows:

- i. constant density jets
- ii. variable density jets
- iii. evaporating sprays
- iv. combusting jets
- v. combusting sprays

The entire investigation was divided into two phases. The first phase considered flows i-iii, while the second phase considered iv and v. Each of these phases is discussed, in turn, in the following.

Further details concerning this portion of the investigation can be found in Refs. 16-18, 35-38, and 46-49.

4.2 Evaporating Sprays

Introduction. In this portion of the study, an experimental apparatus was constructed in order to conduct measurements within isothermal air jets, dense gas jets and an evaporating spray. A variety of measurements were completed for comparison with predictions. Jet flow rates and the total momentum of the jet were measured to provide initial conditions. Profiles of mean velocity, velocity fluctuations and Reynolds stress were measured for all the flows. Mean concentration measurements were completed for the isothermal gas jet and the evaporating spray. Mean temperature and drops size distribution measurements were completed for the evaporating spray. Both theoretical and experimental methods used in this study were checked against earlier work in the literature (76-81).

The major elements of the theory were also developed in this phase of the study. Due to the approach taken in the analysis, each specific case is only distinguished by a new equation of state. Thus subsequent considerations of combusting flows involve little additional analysis.

Apparatus. All testing was done in the same apparatus. The injector (airatomizing nozzle, Spraying Systems Company Model 1/4 J 2050 with a No. 67147 air nozzle) was oriented vertically downward. The test area was 2 m high by 0.92 m square, enclosed with 16 mesh screen. Two linear transversing mechanisms were used to position the nozzle in a horizontal plane. The nozzle could also be moved in the vertical direction, along slides.

Gas flow rates through the injector were metered with critical flow orifices. Freon 11 was used as the spray liquid, its flow rate was measured directly by observing the liquid level displacement in the supply vessel. The liquid flow rate was varied by changing the air pressure over the surface of the liquid. The momentum of the jet was determined directly by impingement on a flat plate, supported by a load cell.

Velocities and turbulence quantities were measured by a single channel laser-Doppler anemometer. The arrangement of the LDA is illustrated in Fig. 21. The single channel instrument was employed for various velocity components and turbulence quantities by changing the orientation of the beams (17,47). Temperatures were measured with a 25 μm OD wires mounted in crossflow from heavier leads spaced 20 mm apart. Overall compositions were obtained by isokinetically sampling the flow with a heated probe and analyzing the sample using a gas chromatograph. Liquid mass flux and the drop size distribution in sprays were obtained using a particle impaction technique.

Three test conditions were considered, an air jet (constant density jet), an SF6 jet (variable density jet) and an evaporating Freon 11 spray. The test conditions are summarized in Table 5.

Theory. The theoretical model assumes an axisymmetric turbulent jet in an infinite stagnant gaseous environment. The spray is treated with LHF approximation. This implies that drop and gas velocities and temperatures are equal at each point in the flow, and that the drops and the vapor are in thermodynamic equilibrium, i.e., that the partial pressure of the vapor is the saturated vapor pressure of the liquid, as long as any liquid is present. The calculations are based on Reynolds averaging the conservation equations. Similar to other models of this type (76), production and dissipation effects due to density fluctuations are ignored. It is also assumed that laminar transport occurs with equal diffusion coefficients, that turbulent species and heat exchange coefficients are equal as well, and that radiation and kinetic heating are negligible.

Under these assumptions, the conservation equations are as follows (17,76):

$$\frac{\partial \bar{\rho} \bar{u}}{\partial x} + \frac{1}{r} \frac{\partial}{\partial r} (r \bar{\rho} \bar{v}^0) = D(\bar{f}) = 0 \quad (1)$$

$$D(\bar{u}) = a(\bar{\rho}_\infty - \bar{\rho}) \quad (2)$$

$$D(k) = \mu_t \left(\frac{\partial \bar{u}}{\partial r} \right)^2 - \bar{\rho} \epsilon \quad (3)$$

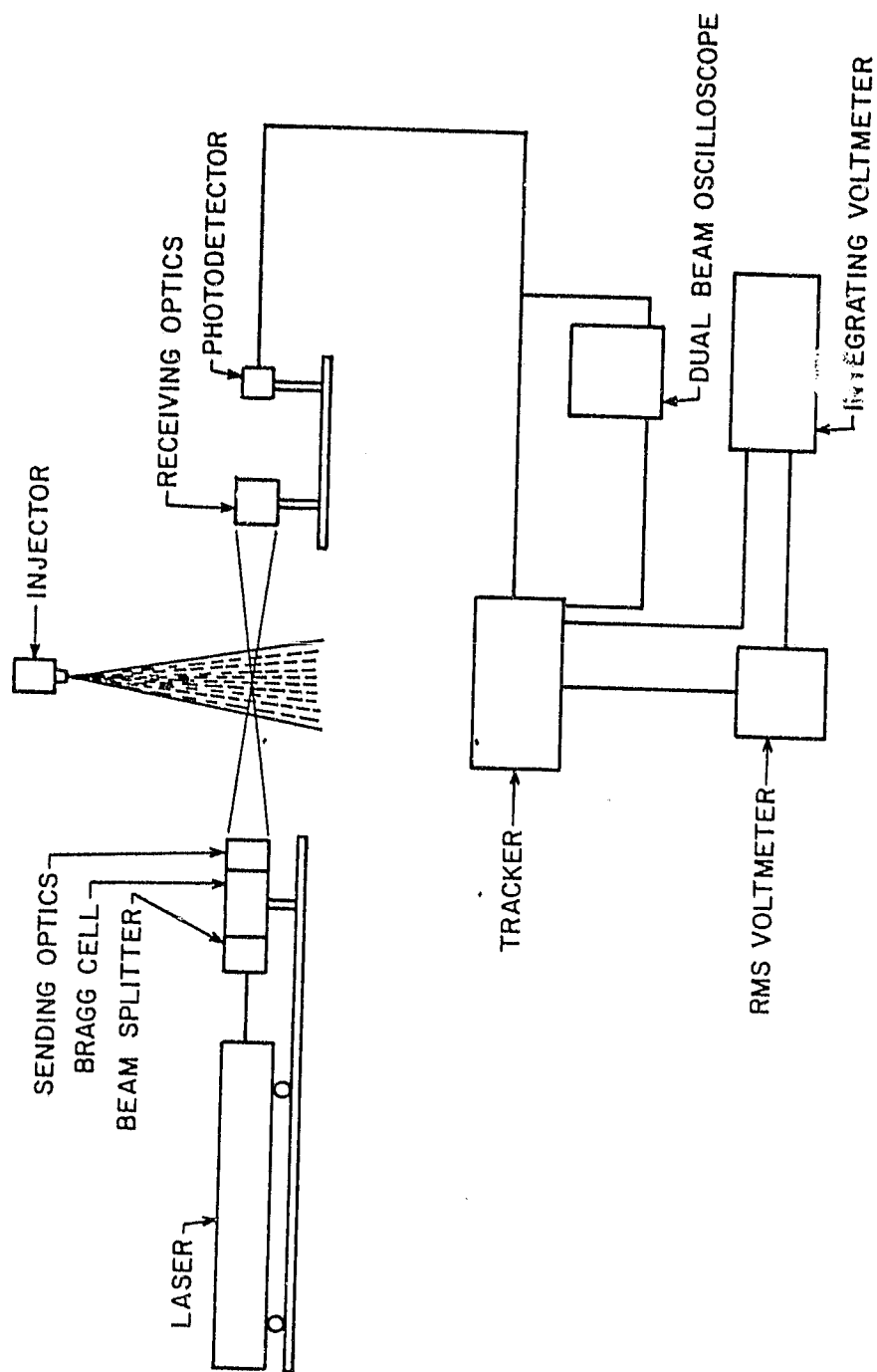


Fig. 21 Schematic diagram of the LDA system for jet and spray measurements.

Table 5

Summary of Test Conditions^a

Case	1	2	3
Injector Fluid	Air	Sulfur Hexafluoride	Freon-11
Injector Flow Rates (g/s)			
Gas	0.467	0.103	0.225
Liquid	0	0	1.548
Injector Pressures (kPa)			
Gas	203	186	211
Liquid	--	--	138
Jet Momentum (N)	0.100	0.0093	0.132
Sauter Mean Diameter ^b (μm)	--	--	29
Initial Velocity (m/s)	214.1	90.30	74.45

^a $T_{\infty} = 296 \text{ K}$, $P_{\infty} = 97 \text{ kPa}$

^bMeasured 203 mm from injector.

$$D(\epsilon) = C_{\epsilon 1} \mu_t \frac{\epsilon}{k} \left(\frac{\partial \bar{u}}{\partial r} \right)^2 - C_{\epsilon 2} \bar{\rho} \frac{\epsilon^2}{k} \quad (4)$$

$$D(g) = C_{g1} \mu_t \left(\frac{\partial \bar{f}}{\partial r} \right)^2 - C_{g2} \bar{\rho} \frac{\epsilon g}{k} \quad (5)$$

where

$$\bar{\rho} \bar{v}^0 = \bar{\rho} \bar{v} + \overline{\rho' v'} \quad (6)$$

$$D(\phi) = \bar{\rho} \bar{u} \frac{\partial \phi}{\partial x} + \bar{\rho} \bar{v}^0 \frac{\partial \phi}{\partial r} - \frac{1}{r} \frac{\partial}{\partial r} \left(r \frac{\mu_t}{\sigma_\phi} \frac{\partial \phi}{\partial r} \right) \quad (7)$$

for $\phi = \bar{u}, \bar{f}, k, \epsilon$ or g . The boundary conditions for these equations are:

$$r = 0, \frac{\partial \phi}{\partial r} = 0; \quad r \rightarrow \infty, \phi = 0 \quad (8)$$

The initial conditions are:

$$x = 0, r < d/2, \bar{u} = \dot{M}_0 / \dot{m}_0, \bar{f} = 1, g = 0, k = k_0, \epsilon = \epsilon_0 \quad (9)$$

where the parameters k_0 and ϵ_0 are assumed to have values appropriate for fully developed flow in tubes. The turbulent viscosity is obtained from the following constitutive equation:

$$\mu_t = C_\mu \bar{\rho} k^2 / \epsilon \quad (10)$$

The model is completed by relating the mixture fraction to other properties of the flow, ρ, Y_i, T , etc. Since f is a passive scalar, local properties are completely determined by the thermodynamic equilibrium state attained during adiabatic mixing of an amount f of injector fluid and $(1-f)$ of ambient fluid, at the ambient pressure. Determination of the equation of state then involves solution of equations for conservation of mass and energy for this mixture along with and phase equilibrium requirements if the mixture is not single-phase.

Figure 22 is an illustration of the equation of state for the Freon 11 spray considered in the experiments. In this case, both air and Freon 11 leave the injector, while the ambient gas is pure air. As the mixture fraction decreases from unity, the concentration of Freon liquid decreases, with all the liquid disappearing at a mixture fraction of 0.33. At this point, the temperature is a minimum and the concentration of Freon 11 vapor is a maximum. The presence of liquid Freon 11 results in a rather nonlinear density variation, particularly at high mixture fractions.

Given the equation of state, the mean value of any scalar quantity (other than \bar{f} , k , ϵ and g) can be determined if the probability density function for f is known as a function of position in the flow. The mean value is then given by

$$\bar{\phi} = \int_0^1 \phi(f) p(f) df \quad (11)$$

where $p(f)$ is the probability density function for f . Following Lockwood and Naguib (76), a clipped Gaussian probability density function was assumed. There are two parameters in this function which must be specified, the most probable value of the distribution and the variance. These parameters are found as a function of position by noting

$$\bar{f} = \int_0^1 f p(f) df, \quad g = \int_0^1 (f - \bar{f})^2 p(f) df \quad (12)$$

Both \bar{f} and g are known from the integration of Eqs. (1)-(10), providing two equations to solve for the unknown parameters in the probability density distribution.

The calculations were performed using a modified version of general-purpose parabolic flow solver, GENMIX (82). The empirical constants appearing in the model were the same as those recommended by Lockwood and Naguib (76). The values are summarized in Table 6. These constants were used in all regions of the flow, including the shear layer near the injector exit.

Results and Discussion. Figure 23 is an illustration of the radial variation of mean axial velocity for an isothermal single-phase jet, a variable density single-phase jet and the evaporating spray. The axial velocity is normalized by the centerline velocity. The radial distance is normalized by the axial distance from the injector so that a direct measure of the width of the flow can be obtained. Experimental results from Wygnanski and Fiedler (78) and Hetsroni and Sokalov (80) are

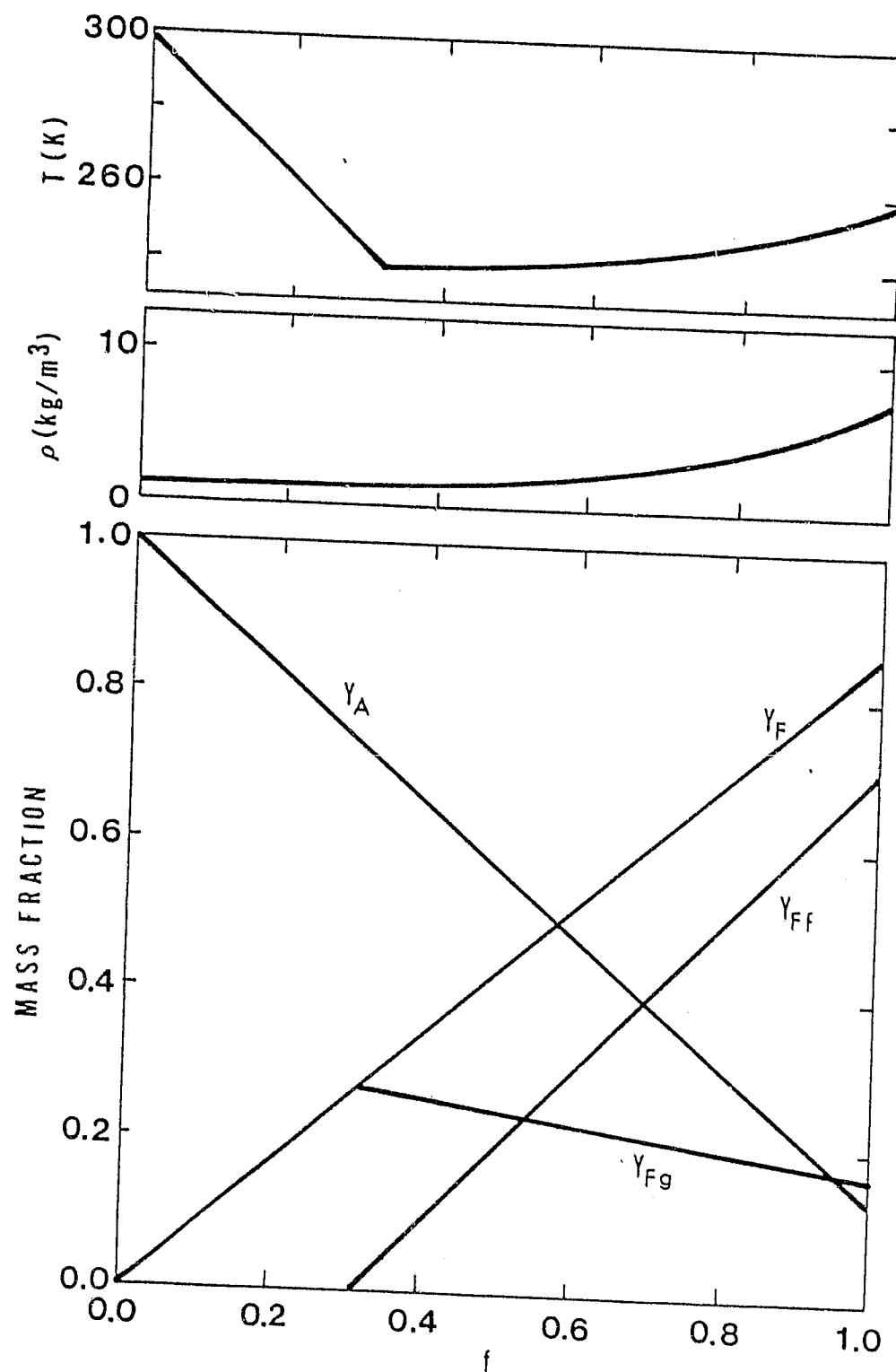


Fig. 22 Equation of state for an evaporating Freon-11 spray.

Table 6

Constants in the Turbulence Model

Constant	Value
C_μ	0.09
C_{ϵ_1}	1.44
$C_{\epsilon_2} = C_{g_2}$	1.89, 1.84 ^a
C_{g_1}	2.8
σ_k	1.0
σ_ϵ	1.3
σ_f	0.7
σ_g	0.7

^aConstant density and variable density flows, respectively.

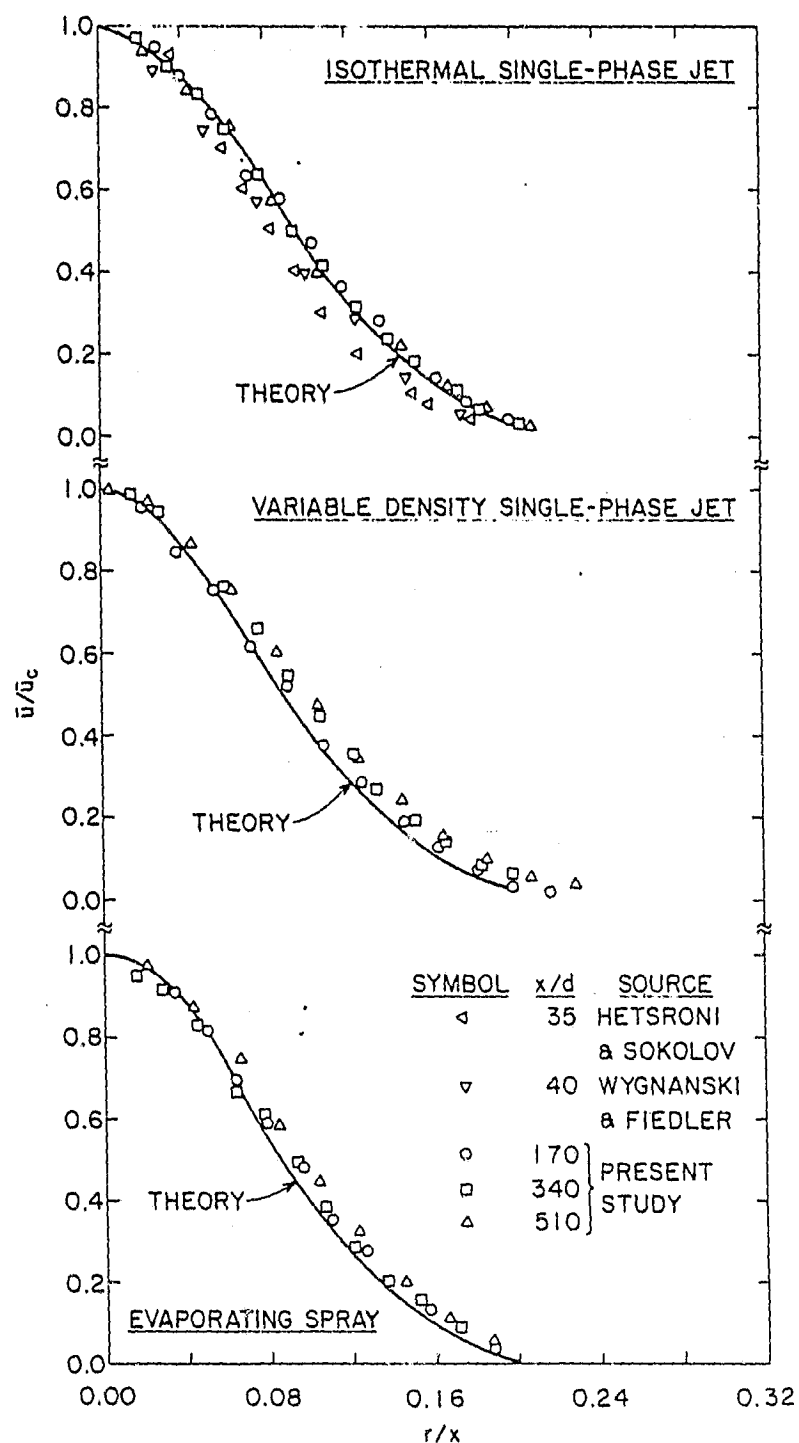


Fig. 23 Theoretical and experimental radial variation of mean axial velocity for constant and variable density gas jets and an evaporating spray.

shown, along with the present measurements. The theoretical results for each case also appear, for comparison with the measurements. In general, the comparison between the measurements of the various studies, and between predictions and measurements, is excellent. Similar agreement was also obtained for mixture fraction.

Figure 24 is an illustration of the radial variation of Reynolds stress for the three flows. The Reynolds stress is normalized by the square of the centerline velocity. The radial coordinate is the same as Fig. 23. The measurements are from Wagnanski and Fiedler (78) and the present investigation. Theory is also illustrated for comparison with the measurements. The scatter of data is greater for this turbulence quantity than for mean quantities. However, the general agreement between predictions and measurements is satisfactory.

Greater differences between the flows become apparent when the axial variation of mean velocity and mixture fraction are considered. Figures 25 and 26 are illustrations of these parameters, as a function of distance from the injector. In addition to the present data, results from other investigations of single and two-phase jets are shown (77-79, 81). Earlier experimental results for air jets are in good agreement with the present measurements. Predictions of the theory are also illustrated for each case. The single-phase jets are modeled quite well, including variable density effects. The discrepancies are larger for the two-phase jets. For the air jet into water, the velocity variation is predicted quite well, but the error is significant for mixture fraction. The method used by Tross (81) to evaluate mixture fraction, tends to underestimate this quantity and the problem could be with the experiments. This flow also has the largest density variation of all the flows considered, and a difficulty with neglecting density fluctuations in the model cannot be ruled out (17,37). The measured variation of mean velocity and mixture fraction for the evaporating spray clearly lags the predictions. Comparisons between predicted and measured liquid fluxes and temperatures also indicated that the flow was developing more slowly than predicted.

Since the other flows were predicted reasonably well by the model, it appeared that slip and loss of thermodynamic equilibrium might be the reason for the errors in the spray predictions. This was examined by completing drop-life-histories in the flow. The life-history calculations considered drops passing along the centerline of the flow with initial conditions corresponding to properties at the injector exit. The local ambient conditions of the drop were obtained from the predictions of the LHF turbulence model. Since computation of drop-life-histories is subject to errors due to uncertainties in the properties to be used in the computations, the calculation procedure was calibrated using experimental results from single drop experiments with well-defined ambient conditions around the test drop.

The results of the drop-life-history calculations are illustrated in Fig. 27. Initial drop diameters of 10, 30 and 50 μm are considered.

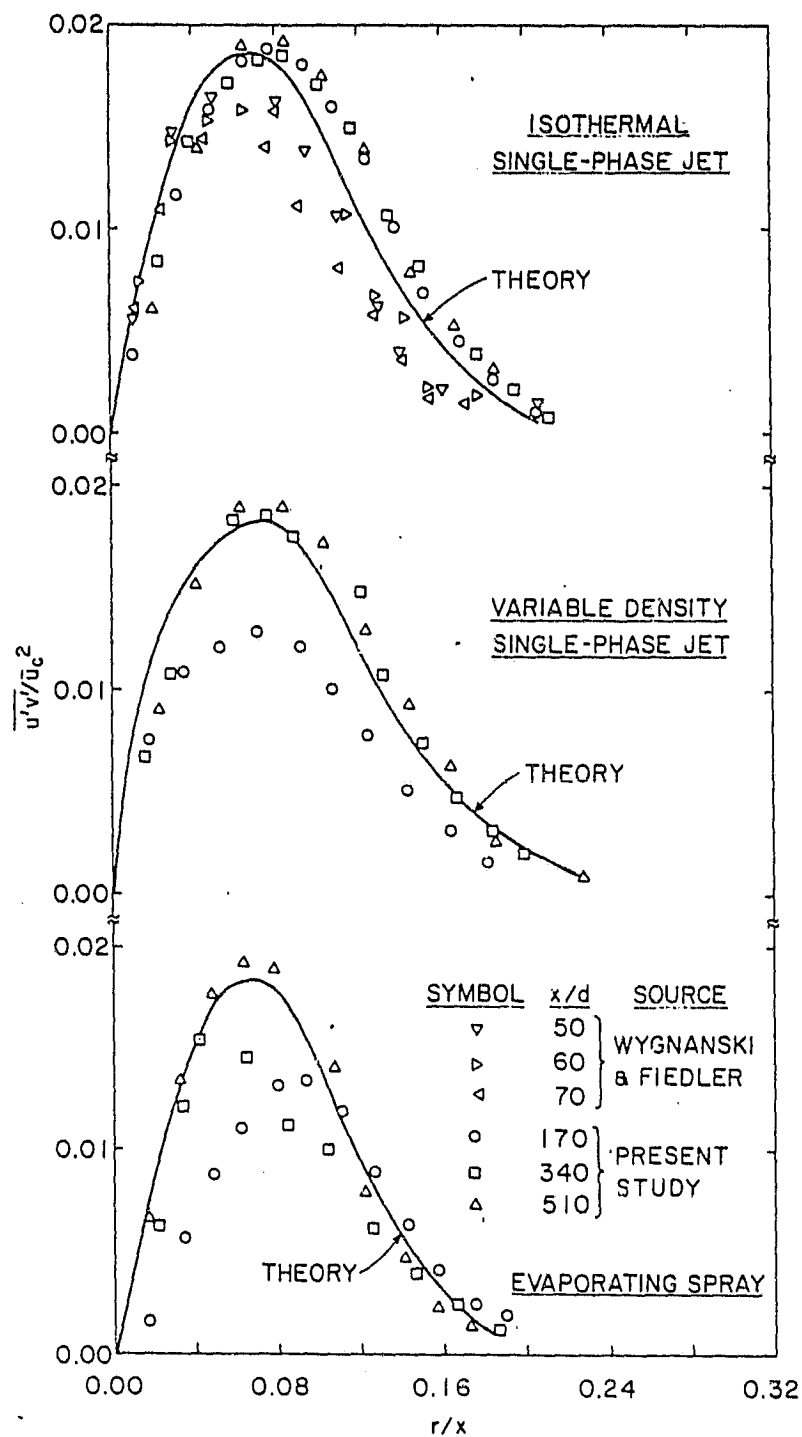


Fig. 24 Theoretical and experimental radial variation of Reynolds stress for constant and variable density gas jets and an evaporating spray.

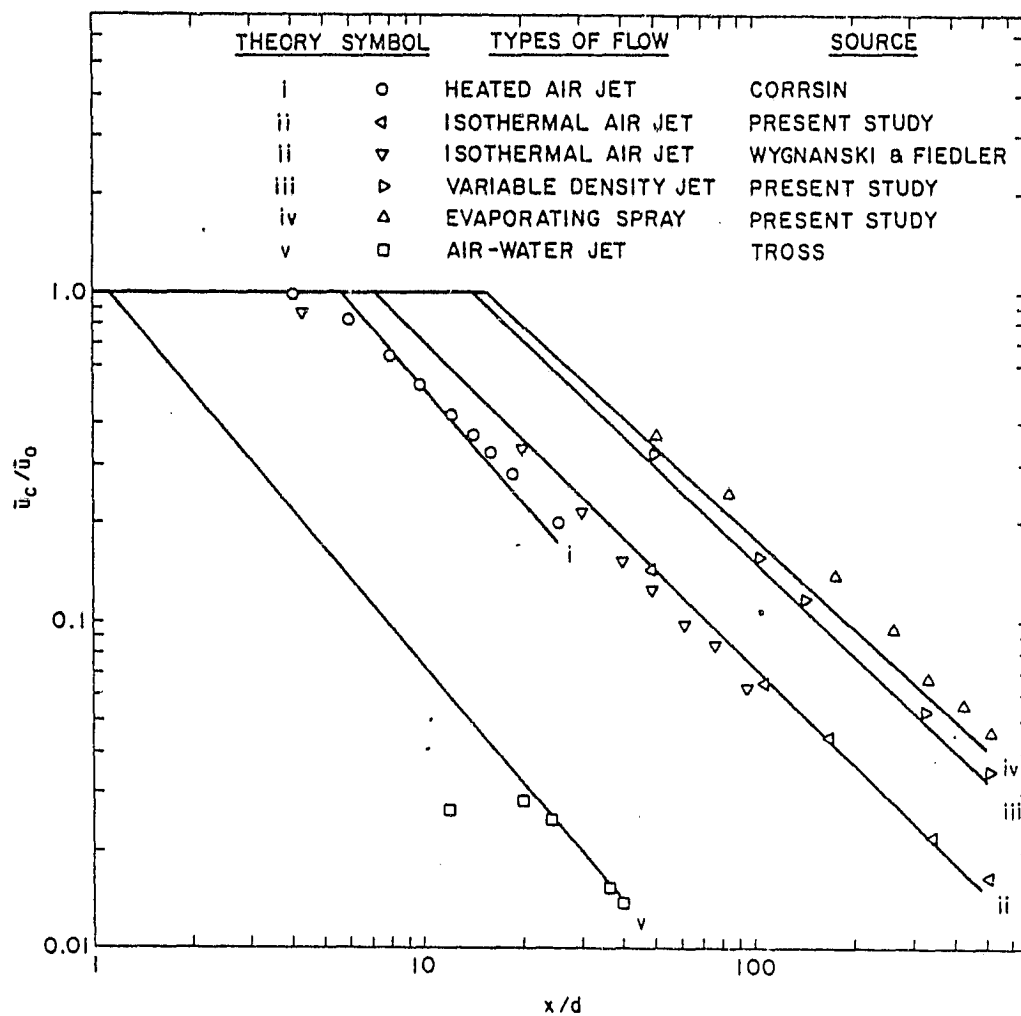


Fig. 25 Theoretical and experimental variation of mean centerline velocity for various gas jets and an evaporating spray.

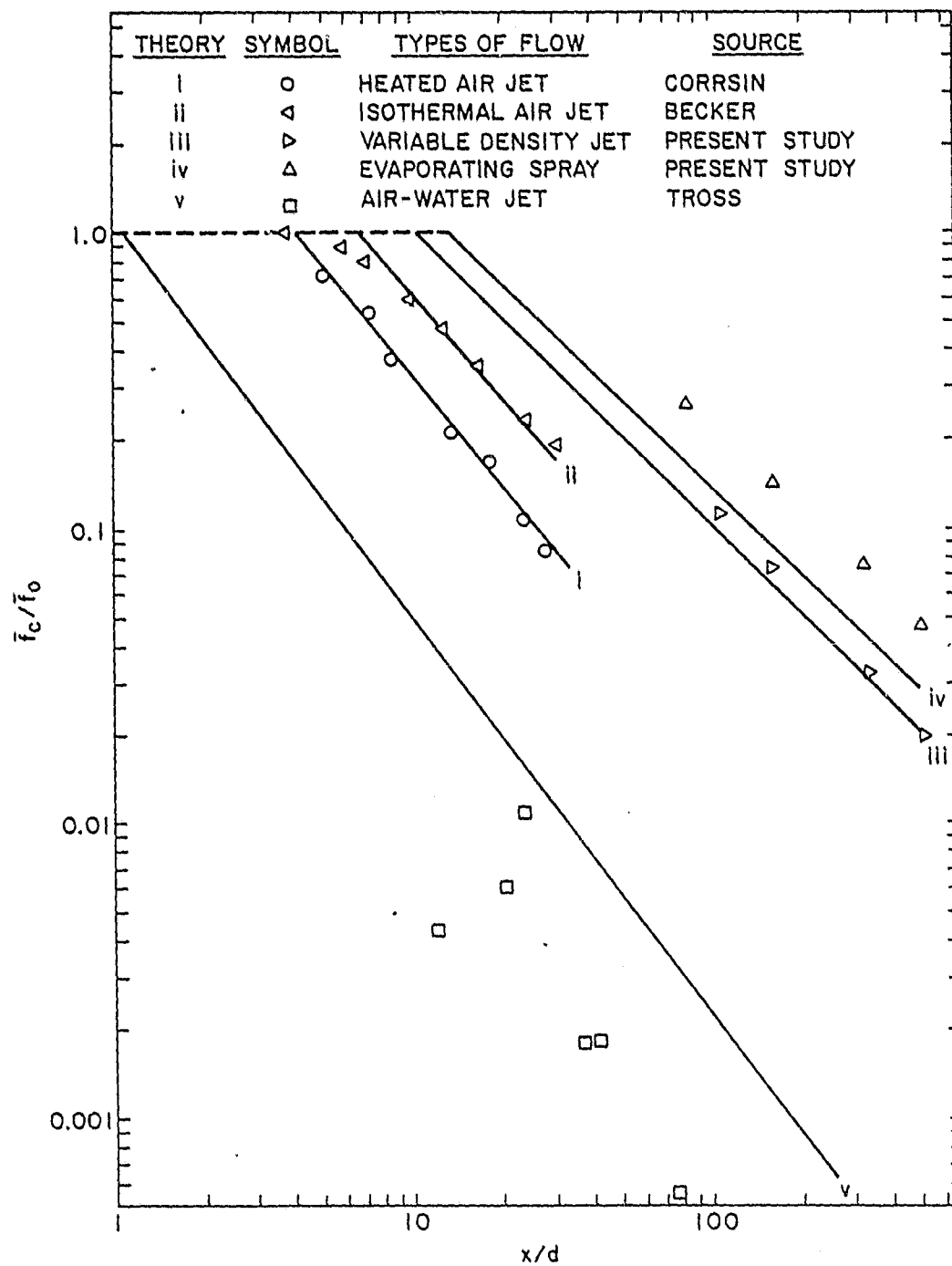


Fig. 26 . Theoretical and experimental variation of mean centerline mixture fraction for various gas jets and an evaporating spray.

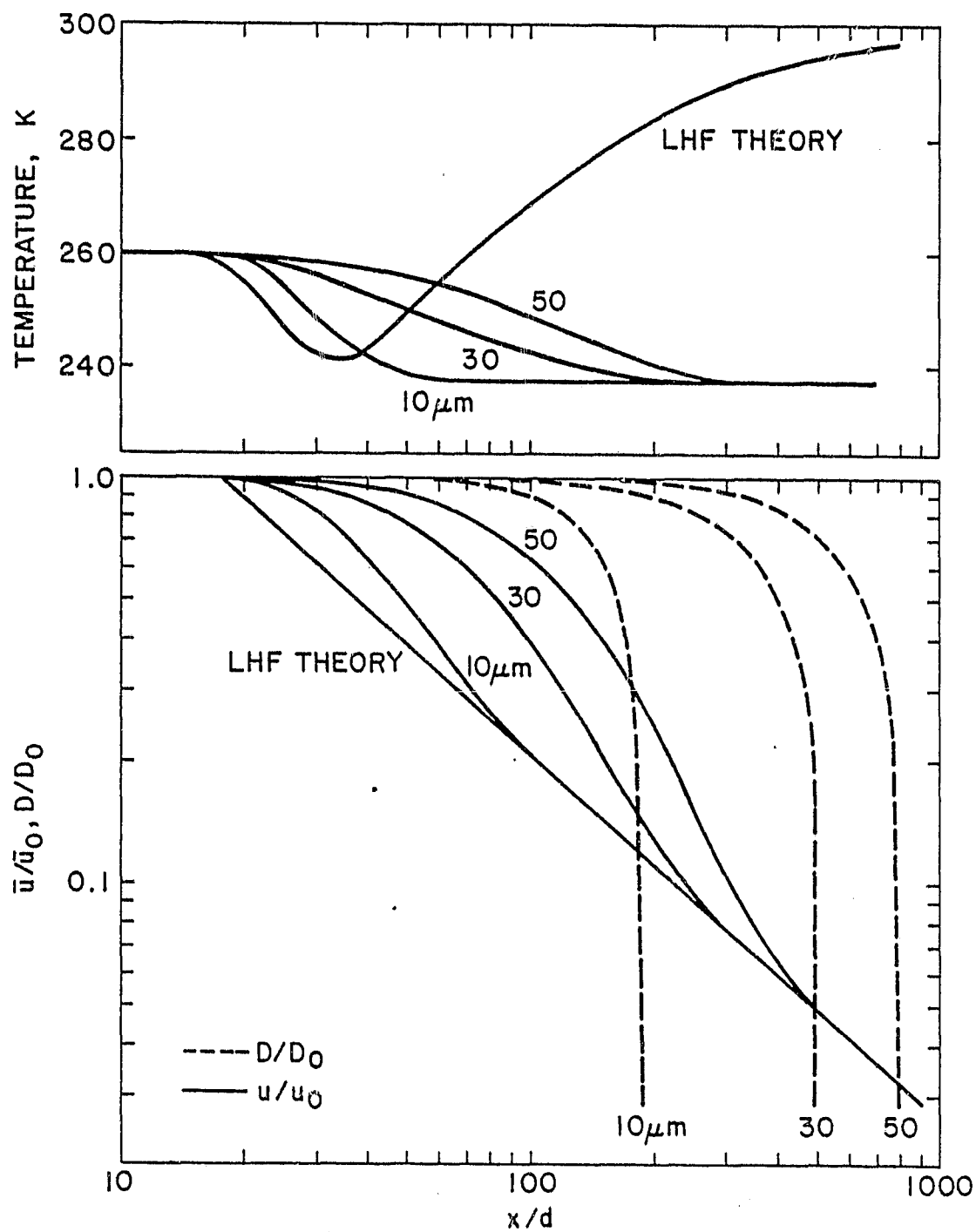


Fig. 27 Predicted drop-life histories in an evaporating spray.

The diameter, velocity and temperature of the drop, and the velocity and temperature of the gas at the centerline of the spray, are given as a function of position from the injector. The drop velocities clearly decrease less rapidly than the gas velocities. Appreciable levels of slip occur in the region just downstream of the potential core of the jet. There are also significant differences in the temperatures of the two phases. The temperature errors are largest in the downstream region, where the gas temperature tends to increase while the drop temperature tends to approach a wet-bulb value. The life-history calculations indicate that drops are present for values of x/d_0 greater than 500, which agrees with experimental observations. It appears that the spray considered in this investigation would have to have initial drop diameters less than $10\text{ }\mu\text{m}$, in order to obtain quantitative accuracy with the LHF model.

Conclusions. The model provides excellent predictions of mean quantities in single-phase constant and variable density jets. The agreement between predicted and measured turbulence quantities in single-phase jets was satisfactory. The model provided useful qualitative results for the spray, but slip and loss of thermodynamic equilibrium limited the quantitative predictions of the LHF model, even for a spray having a Sauter mean diameter of $29\text{ }\mu\text{m}$ at atmospheric pressure (maximum errors were in the range 20-40% for axial variations of mean velocity and mixture fraction). Analysis of drop-lift histories suggests that a Sauter mean diameter less than $10\text{ }\mu\text{m}$ would be required for quantitative accuracy at these conditions. These small sizes are needed due to the relatively rapid development of the flow, resulting from the relatively small injector diameter.

Since injector diameters are generally small, this finding implies that accurate analysis of most practical sprays will require models which allow for slip and finite rate processes between the phases. The LHF model is still of value in cases where the necessary information on spray characteristics is limited, reducing the potential accuracy of slip models. There are relatively few parameters to be prescribed for the LHF model, other than a conventional thermodynamic prediction for the equation of state. The results provide a lower bound for spray operation - since actual sprays tend to develop more slowly than the LHF predictions. Conducting drop life-history calculations, using the LHF model to prescribe the drop environment, is a convenient means of evaluating the potential accuracy of LHF predictions.

4.3 Spray Combustion

Introduction. The final stage of this investigation considered the application of the LHF model to combusting sprays. Two cases were considered, a spray from an air-atomizing injector at atmospheric pressure and a spray from a pressure atomizing injector at high pressures. The former case is a potential application of the LHF model, due to the small drop diameters produced with air atomizing injectors and the relatively large flame length at atmospheric pressure (similar to the experimental conditions of Onuma and Ogasawara (73)). LHF models also show promise at high pressures, since the densities of the two phases approach one another. The LHF method also provides a

relatively simple approach for treating combustion near the thermodynamic critical point, where difficulties are encountered with drop-life-history computations.

Apparatus. Tests at atmospheric pressure were conducted in the apparatus discussed in Section 4.2. The major difference was that the injector faced upward. Test conditions involved repeating the air and sulfurhexafluoride tests, discussed earlier; and conducting tests in a combusting propane gas jet and a combusting pentane-fueled spray. The flames were stabilized at the injector exit using four small capillary flames fueled with hydrogen. Measurements in the combusting jets were limited to mean axial velocities, using the LDA, and gas temperatures, using 50 μm diameter Pt/Pt-10% Rh thermocouples. The thermocouple wires were shielded in the spray flame, in order to prevent impingement of drops on the junction. The test conditions for the combusting jets at atmospheric pressure are summarized in Table 7.

Tests at elevated pressures were conducted in the apparatus pictured in Fig. 28. The environment of the spray consisted of air, under pressure, within the test chamber. Since only a limited quantity of air was present, the injector was operated for a relatively short time, in order to reduce vitiation of its atmosphere. The test duration was long enough, however, to insure steady combustion.

Liquid fuel for the test was placed in a tube loop within the chamber. The fuel was forced through the injector by opening a solenoid valve to a capacitance chamber, maintained at a pressure greater than the test chamber pressure. The test terminated when all the fuel in the loop had passed through the injector. The injector was a Spraying Systems Company straight hole injector with a model 0.000009 solid stream tip. The spray was ignited and stabilized by a hot wire passing close to the injector exit. The combustion process was observed through windows in the test chamber. Motion picture shadowgraphs were obtained in order to measure the boundaries of the spray. Dark-field motion pictures were obtained for flame shape measurements. The high pressure test conditions are summarized in Table 8.

Theory. A preliminary version of the LHF model for combusting sprays was based on an integral model of the flow and low pressure thermodynamics (16,46). This earlier model has been superceded by the k- ϵ -g turbulence model, using high pressure thermodynamics, and will not be discussed here.

The basic turbulence model remains unchanged from the version considered in Section 4.2. Consideration of combusting sprays only requires the construction of a new equation of state. Under the LHF assumption, complete thermodynamic equilibrium is specified for each point in the flow. At low mixture fractions, where the ideal gas equation of state is valid, equilibrium was determined from the

Table 7

Summary of Test Conditions for Combusting Jets
at Atmospheric Pressure^a

Fuel	n-Propane	n-Pentane ^b
Fuel State	vapor	liquid
Fuel flow rate (g/s)	0.18	0.35
Air flow rate (g/s)	-	0.080
Injector pressures (kPa)		
Gas side	131.0	120.6
Liquid side	-	137.9
Injector Thrust (mN)	15.6	5.00
Jet Velocity (m/s)	88.7	11.6

^a Ambient conditions 296 K, 97 kPa, injector diameter 1.194 mm, injector oriented vertically upward.

^b Sauter mean diameter 35 μm measured at $x/d = 170$, at the centerline, in cold flow.

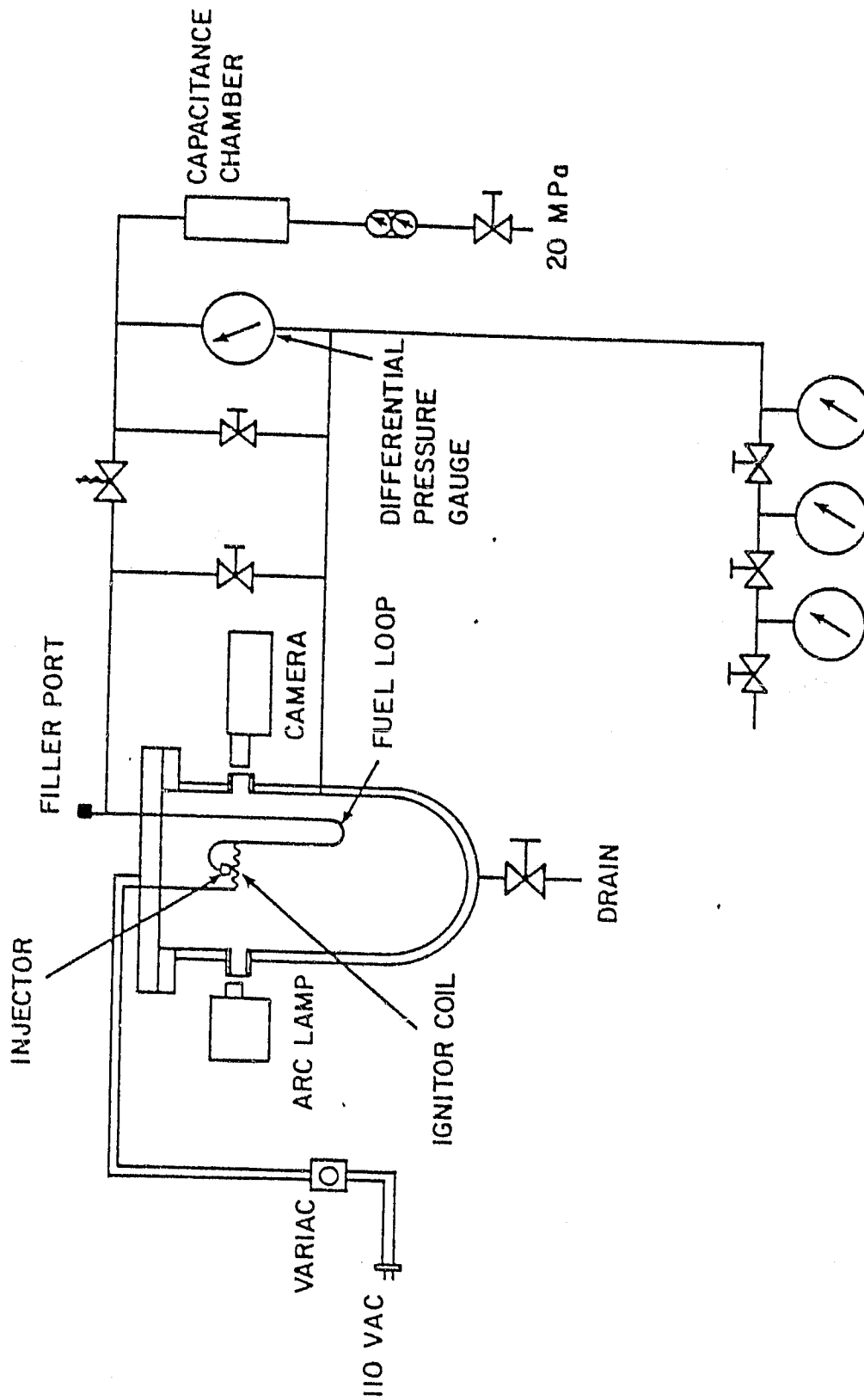


Fig. 28 Sketch of the high pressure spray combustion apparatus.

Table 8
Summary of Test Conditions for Combusting
Sprays in High Pressure Air

Fuel	n-pentane
Sauter mean diameter	28 μm^{a}
Maximum drop diameter	79 μm^{a}
Spray velocity	68.5 m/s
Ambient temperature	20 C
Ambient pressure	3, 6 and 9 MPa

^aCalculated, cf Ref. 16

NASA CEC 72 program (83). At high mixture fractions and high pressures, compressibility and solubility effects are important and were treated using the Redlich-Kwong equation of state (57). For hydrocarbons, some decision must be made concerning soot formation at high mixture fractions. This was handled by assuming that no soot was formed at temperatures below 1000 K.

An illustration of a typical equation of state for a combusting spray appears in Fig. 29. The system involves the combustion of an n-pentane spray, from a pressure atomizing injector, in air. This pressure is 6 MPa which is roughly 1.8 times the critical pressure of pure n-pentane. High pressure effects are evident at large mixture fractions. In the region where liquid is present, $f < 0.8$, the variation of all species concentrations is nonlinear. This is due to the fact that significant quantities of gas are dissolved in the liquid phase. Near the stoichiometric mixture ratio, $f = 0.066$, gas temperatures reach a maximum, the density is a minimum, and the concentration of oxygen and fuel approach zero. For the complete range of mixture fractions, the density varies almost two orders of magnitude.

Results and Discussion. Throughout all calculations, the empirical parameters used in the model were not changed from the values given in Table 6. Only the equation of state changes from case to case.

The mean velocities and temperatures measured along the centerline of the combusting gas jet are illustrated in Fig. 30. The predictions of the theory are also presented on the plot. The agreement between theory and experiment is excellent. The comparison was similar for profiles of mean velocity and temperature in the radial direction. Based on these results, it is clear that the model is capable of handling combustion processes in gas flows, with no additional modification of constants.

The comparison between predictions and measurements for the combusting n-pentane spray at atmospheric pressure is illustrated in Fig. 31. Mean velocities and temperatures are plotted as a function of distance from the injector. In this case, there is evidence of the model overestimating the rate of development of the flow. There was not sufficient time available during the current investigation to complete calibrated drop-like-histories for this case. However, the injector was the same as for the evaporating spray, and operating conditions are similar, drop sizes, length of process, rate of decay of mean velocity, etc. Therefore, effects of slip, like those pictured in Fig. 27, would be expected for the combusting spray illustrated in Fig. 31. Similar to the case of an evaporating spray, the radial variation of mean velocity and temperature was predicted reasonably well.

The comparison between the predictions of the model and spray penetration length measurements for the high pressure combusting pentane spray are summarized in Table 9. The degree of agreement

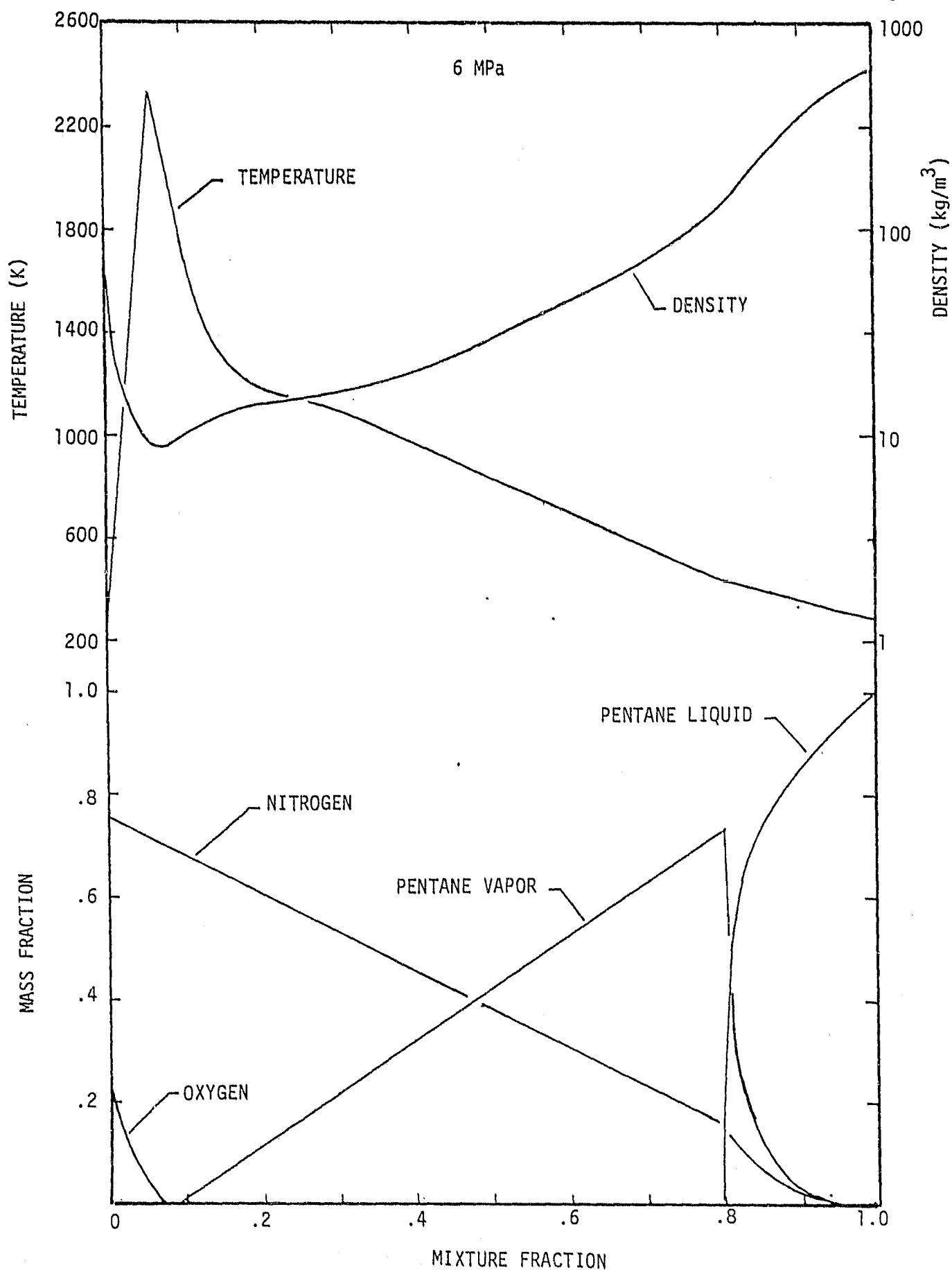


Fig. 29 Equation of state for a combustng n-pentane spray in air at 6 MPa.

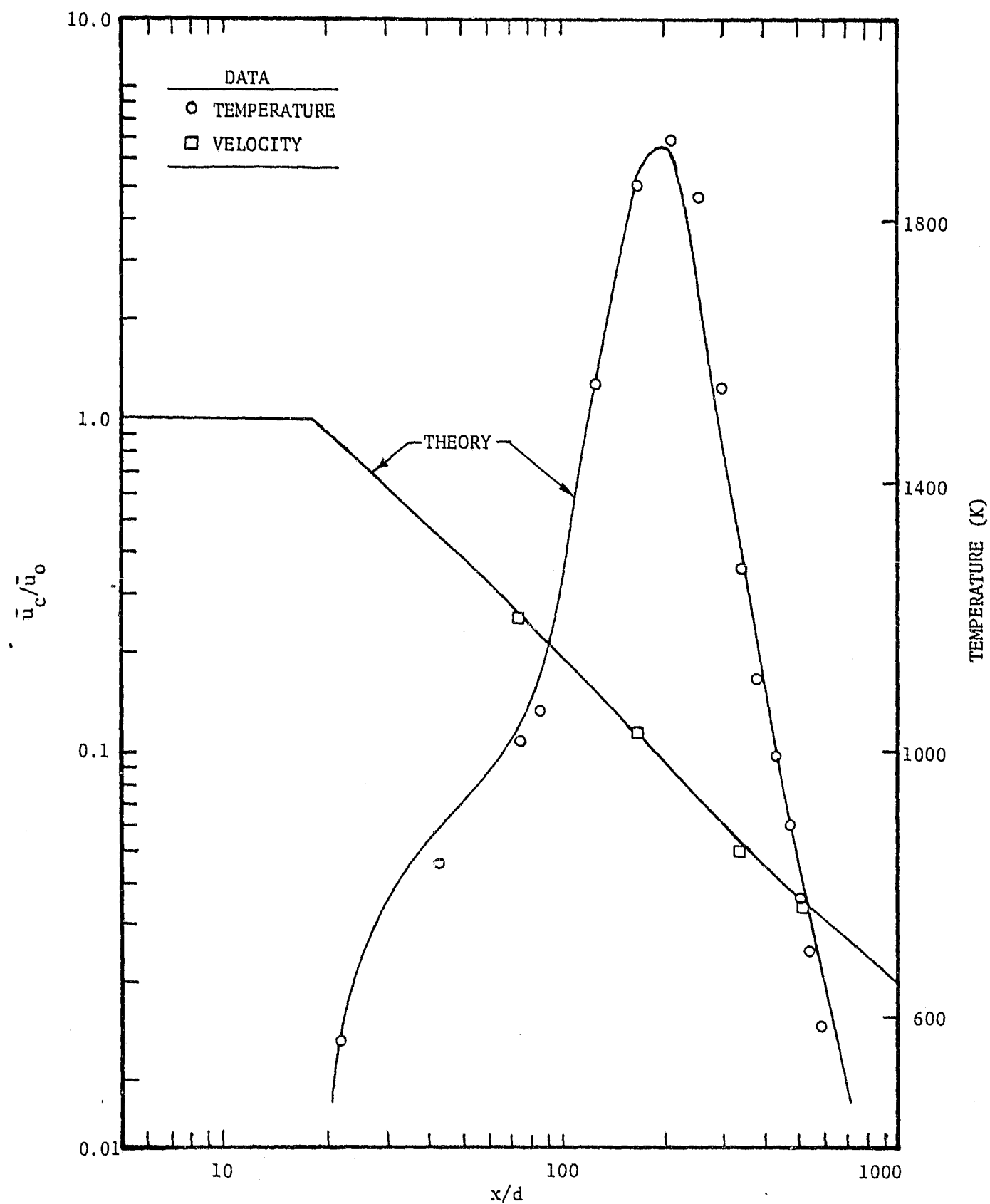


Fig. 30 Theoretical and experimental mean velocity and temperature variation along the centerline of a combustng gas jet at atmospheric pressure.

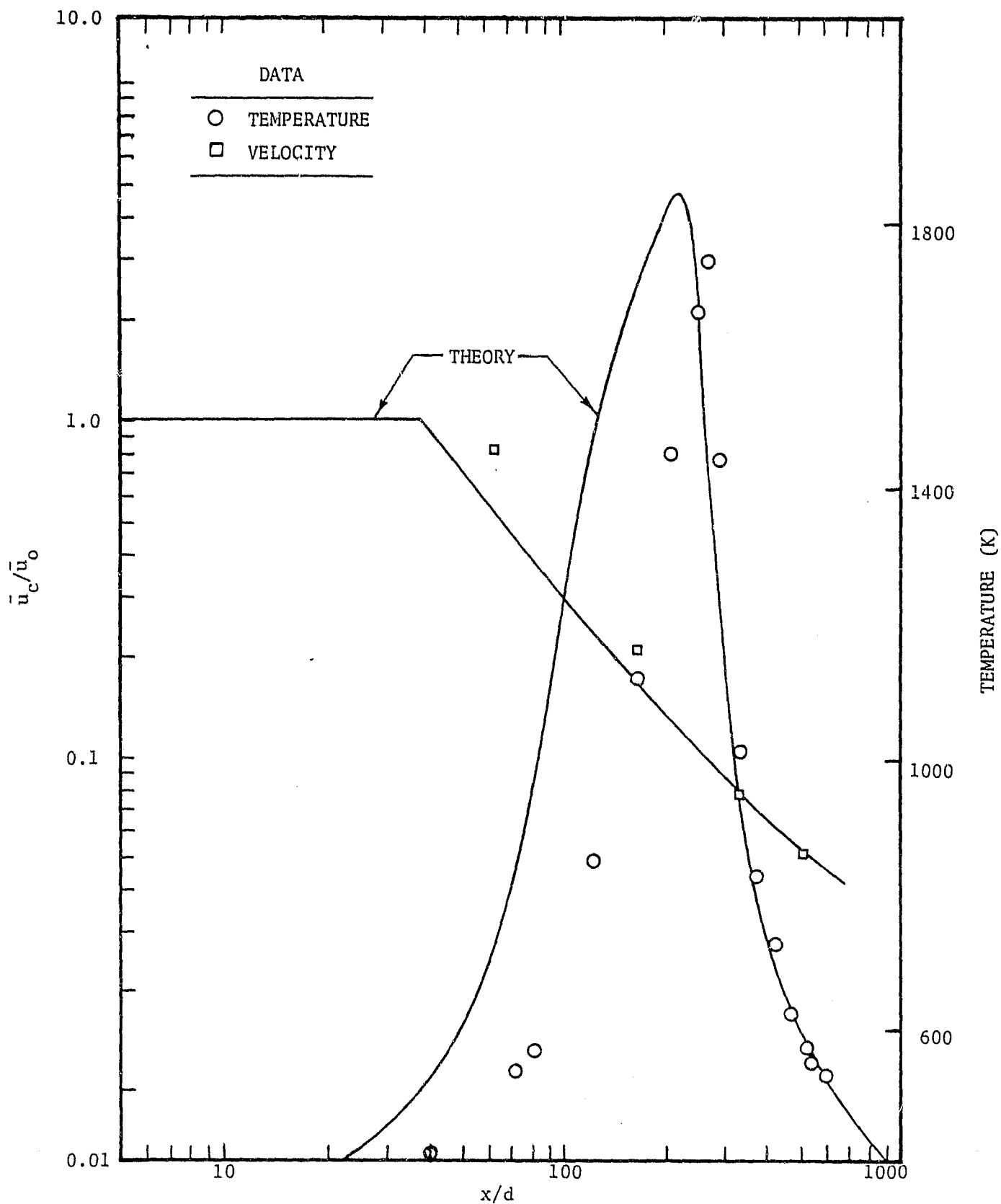


Fig. 31 Theoretical and experimental mean velocity and temperature variation along the centerline of a combustive spray at atmospheric pressure.

Table 9

Comparison of Measured and Predicted Spray
Penetration Lengths at High Pressures^a

Pressure (Mpa)	<u>Spray Length/Injector Diameter</u>	
	Measured	Predicted
3	132	128
6	119	79
9	100	67

^aTest conditions appear in Table 8.

between predictions and measurements is encouragingly good. However, spray penetration length is not as sensitive a measure as mean temperature and velocity comparisons. Therefore, further experimental results are needed to provide a convincing demonstration of the application of the LHF model at high pressures. Drop-life-history calculations should also be completed, in order to more rigorously assess the effects of slip and loss of chemical equilibrium between the phases.

Conclusions. The model was very effective in predicting mean velocities and temperatures in a combustng gas jet. An important feature of this comparison is that the constants used in the model are the same as those generally in use for turbulent jet computations (76). These constants were evaluated again in the present investigation by systematic comparison with measurements for constant density and variable density jets. The fact that no additional parameter was adjusted to obtain the comparison shown in Fig. 30, other than a standard chemical equilibrium calculation to obtain an equation of state, suggests that the model has some potential for a priori predictions.

There was evidence of slip effects for the atmospheric pressure spray, although the analysis did provide qualitative agreement with the measurements. The predictions of spray penetration lengths for high pressure combustion were reasonably good, although this parameter is a relatively coarse measure of model accuracy. Further experimental results and the completion of drop-life-history calculations are needed for a more thorough assessment of the LHF model for combustng sprays.

The advantage of the approach outlined here is that there is a minimum of "art" required to complete a prediction. Only the injector geometry, flow rate, momentum and the initial state of the reactants must be specified. An equation of state must be constructed, using conventional equilibrium thermodynamics. All other parameters of the solution are fixed. The solution yields a qualitatively correct picture of the combustion process, at least in the cases considered to date. However, the solution tends to overestimate the rate of development of the flow, since finite rate processes between the phases are ignored. Thus, the results of the LHF prediction represent a lower bound, all real sprays will develop more slowly. Completing drop-life-history calculations, using the LHF model results to estimate local conditions within the spray, provides a systematic means of evaluating the potential accuracy of the LHF model for a given application.

REFERENCES

Reports under this Contract

1. G.M. Faeth, D.P. Dominicis and D.R. Olson, "An Investigation of Near Critical and Super-Critical Burning of Fuel Droplets," NASA CR-72314, Department of Mechanical Engineering, The Pennsylvania State University, University Park, PA, September, 1967.
2. D.P. Dominicis, "An Experimental Investigation of Near Critical and Supercritical Burning of Bipropellant Droplets," NASA CR-72399, Department of Mechanical Engineering, The Pennsylvania State University, University Park, PA, April, 1968.
3. G.M. Faeth, "An Investigation of Near Critical and Supercritical Burning of Fuel Droplets," Second Annual Report under NASA Grant NGR 39-009-077, Department of Mechanical Engineering, The Pennsylvania State University, University Park, PA, September, 1968.
4. G.M. Faeth and R.S. Lazar, "Bipropellant Droplet Burning Rates and Lifetimes in a Combustion Gas Environment," NASA CR-72622, Department of Mechanical Engineering, The Pennsylvania State University, University Park, PA, December, 1969.
5. G.M. Faeth, "An Investigation of Near Critical and Supercritical Burning of Fuel Droplets," Third Annual Report under NASA Grant NGR 39-009-077, Department of Mechanical Engineering, The Pennsylvania State University, University Park, PA, January, 1970.
6. G.M. Faeth, "1970 Annual Report on the Investigation of Critical Pressure Burning of Fuel Droplets," NASA CR-72834, Department of Mechanical Engineering, The Pennsylvania State University, University Park, PA, January, 1971.
7. C.B. Allison, "Hybrid and Decomposition Combustion of the Hydrazine Fuels," NASA CR-72977, Department of Mechanical Engineering, The Pennsylvania State University, University Park, PA, July, 1971.
8. C.B. Allison, G.S. Canada and G.M. Faeth, "1971 Annual Report on the Investigation of Critical Burning of Fuel Droplets," NASA CR-120879, Department of Mechanical Engineering, The Pennsylvania State University, University Park, PA, January, 1972.
9. C.B. Allison, G.S. Canada and G.M. Faeth, "1972 Annual Report on the Investigation of Critical Burning of Fuel Droplets," NASA CR-121113, Department of Mechanical Engineering, The Pennsylvania State University, University Park, PA, January, 1973.

10. C.B. Allison, G.S. Canada and G.M. Faeth, "1973 Annual Report on Investigation of Critical Burning of Fuel Droplets," Report under NASA Grant NGR 39-009-077, Department of Mechanical Engineering, The Pennsylvania State University, University Park, PA, January, 1974.
11. G.S. Canada, "High Pressure Combustion of Liquid Fuels," NASA CR-134540, Department of Mechanical Engineering, The Pennsylvania State University, University Park, PA, January, 1974.
12. C.B. Allison, "Burning Rate Response of Liquid Monopropellants to Imposed Pressure Oscillations," NASA CR-134541, Department of Mechanical Engineering, The Pennsylvania State University, University Park, PA, January, 1974.
13. G.M. Faeth and S. Chanin, "1974 Annual Report on Investigation of Critical Burning of Fuel Droplets," NASA CR-134793, Department of Mechanical Engineering, The Pennsylvania State University, University Park, PA, February, 1975.
14. S.P. Chanin and G.M. Faeth, "Oscillatory Combustion of Liquid Monopropellant Drops," NASA CR-134983, Department of Mechanical Engineering, The Pennsylvania State University, University Park, PA, March, 1976.
15. S.P. Chanin, A.J. Shearer and G.M. Faeth, "1975 Annual Report on Investigation of Critical Burning of Fuel Drops," NASA CR-135006, Department of Mechanical Engineering, The Pennsylvania State University, University Park, PA, March, 1976.
16. A.J. Shearer and G.M. Faeth, "Combustion of Liquid Sprays at High Pressures," NASA CR-135210, Department of Mechanical Engineering, The Pennsylvania State University, University Park, PA, March, 1977.
17. A.J. Shearer and G.M. Faeth, "Evaluation of a Locally Homogeneous Model of Spray Evaporation," NASA CR-3198, Department of Mechanical Engineering, The Pennsylvania State University, University Park, PA, March, 1979.
18. C-P. Mao, G.A. Szekely, Jr. and G.M. Faeth, "Evaluation of a Locally Homogeneous Flow Model of Spray Combustion," NASA CR-3202, Department of Mechanical Engineering, The Pennsylvania State University, University Park, PA, July, 1979.

Papers under this Contract

19. G.M. Faeth and D.P. Dominicus, "An Experimental Study of Bipropellant Droplet Combustion at High Pressures," Proc. 4th ICRPG Combustion Conference, CPIA Pub. No. 162, Vol. 1, pp. 211-219, December, 1967.

20. G.M. Faeth, D.P. Dominicus, J.F. Tulpinsky and D.R. Olson, "Supercritical Droplet Combustion," Twelfth Symposium (International) on Combustion, The Combustion Institute, Pittsburgh, PA, pp. 9-18, 1969.
21. G.M. Faeth, R.S. Lazar and J.F. Tulpinsky, "A Study of Droplet Gasification and Combustion at High Pressures," Proc. 5th ICRPG Combustion Conference, CPIA Pub. No. 183, pp. 283-291, December, 1968.
22. G.M. Faeth and R.S. Lazar, "Bipropellant Droplet Burning Rates and Lifetimes in a High Temperature Environment," Proc. 6th ICRPG Liquid Propellant Combustion Instability Conference, CPIA Publication No. 192, Vol. 1, pp. 51-60, December, 1969.
23. R.S. Lazar and G.M. Faeth, "Bipropellant Droplet Combustion in the Vicinity of the Critical Point," Thirteenth Symposium (International) on Combustion, The Combustion Institute, Pittsburgh, PA, pp. 743-753, 1971.
24. R.S. Lazar and G.M. Faeth, "Gas Solubility Effects During High Pressure Liquid Propellant Combustion," Proc. 7th JANNAF Liquid Propellant Combustion Instability Meeting, CPIA Publication 204, Vol. 1, pp. 543-552, February, 1971.
25. G.M. Faeth and R.S. Lazar, "Fuel Droplet Burning Rates in a Combustion Gas Environment," AIAA J., Vol. 9, No. 11, pp. 2165-2171, 1971.
26. C.B. Allison and G.M. Faeth, "Hybrid and Decomposition Combustion of Hydrazine, MMH and UDMH as Droplets," Proc. 8th JANNAF Liquid Propellant Combustion Instability Meeting, CPIA Publication No. 220, Vol. 1, pp. 535-544, November, 1971.
27. C.B. Allison and G.M. Faeth, "Decomposition and Hybrid Combustion of Hydrazine, MMH and UDMH as Droplets in a Combustion Gas Environment," Combustion and Flame, Vol. 19, No. 2, pp. 213-226, 1972.
28. G.S. Canada and G.M. Faeth, "Fuel Droplet Burning Rates at High Pressures," Fourteenth Symposium (International) on Combustion, The Combustion Institute, Pittsburgh, PA, pp. 1345-1354, 1973.
29. C.B. Allison and G.M. Faeth, "Response of a Burning Liquid Fuel to Imposed Pressure Oscillations," Proc. 10th JANNAF Combustion Meeting, CPIA Publication No. 243, Vol. III, pp. 59-66, December, 1973.
30. G.S. Canada and G.M. Faeth, "Combustion of Liquid Fuels in a Flowing Combustion Gas Environment at High Pressure," Fifteenth Symposium (International) on Combustion, The Combustion Institute, Pittsburgh, PA, pp. 501-512, 1975.

31. C.B. Allison and G.M. Faeth, "Open-Loop Response of a Burning Liquid Monopropellant," AIAA J., Vol. 13, No. 10, pp. 1287-1294, 1975.
32. S.P. Chanin and G.M. Faeth, "Oscillatory Combustion of Monopropellant Droplets," AIAA J., Vol. 15, No. 3, pp. 346-353, 1977.
33. S.P. Chanin and G.M. Faeth, "Combustion Response of Monopropellant Drops and Sprays," Proc. 13th JANNAF Combustion Meeting, CPIA Publication No. 281, Vol. III, pp. 109-118, December, 1976.
34. G.M. Faeth, "Current Status of Droplet and Liquid Combustion," Prog. Energy Combust. Sci., Vol. 3, pp. 191-224, 1977.
35. A.J. Shearer, H. Tamura and G.M. Faeth, "Evaluation of a Locally Homogeneous Model of Spray Evaporation and Combustion," AIAA Paper No. 78-1042, AIAA/SAE 14th Joint Propulsion Conference, Las Vegas, NV, July, 1978.
36. G.M. Faeth, "Spray Combustion Models - A Review," AIAA Paper No. 79-0293, AIAA 17th Aerospace Sciences Meeting, New Orleans, LA, January, 1979.
37. A.J. Shearer, H. Tamura and G.M. Faeth, "Evaluation of a Locally Homogeneous Flow Model of Spray Evaporation," J. Energy, in press.
38. C-P. Mao, G.A. Szekely, Jr. and G.M. Faeth, "Evaluation of a Locally Homogeneous Flow Model of Spray Combustion," submitted for publication.

Theses under this Contract

39. D.P. Dominicus, "An Experimental Investigation of Near Critical and Supercritical Burning of Bipropellant Droplets," M.S. Thesis, Department of Mechanical Engineering, The Pennsylvania State University, University Park, PA, June, 1968.
40. J.F. Tulpinsky, "Supercritical Bipropellant Droplet Combustion," M.S. Thesis, Department of Mechanical Engineering, The Pennsylvania State University, University Park, PA, March, 1969.
41. R.S. Lazar, "Bipropellant Droplet Combustion in the Vicinity of the Critical Point," Ph.D. Thesis, Department of Mechanical Engineering, The Pennsylvania State University, University Park, PA, September, 1970.
42. C.B. Allison, "Hybrid and Decomposition Combustion of Hydrazine Fuels," M.S. Thesis, Department of Mechanical Engineering, The Pennsylvania State University, University Park, PA, September, 1971.
43. C.B. Allison, "Burning Rate Response of Liquid Monopropellants to Imposed Pressure Oscillations," Ph.D. Thesis, Department of Mechanical Engineering, The Pennsylvania State University, University Park, PA, March, 1974.

44. G.S. Canada, "High Pressure Combustion of Liquid Fuels," Ph.D. Thesis, Department of Mechanical Engineering, The Pennsylvania State University, University Park, PA, March, 1974.
45. S.P. Chanin, "Oscillatory Combustion of Liquid Monopropellant Droplets," M.S. Thesis, Department of Mechanical Engineering, The Pennsylvania State University, University Park, PA, June, 1976.
46. A.J. Shearer, "High Pressure Spray Combustion in a Stagnant Environment," M.S. Thesis, Department of Mechanical Engineering, The Pennsylvania State University, University Park, PA, August, 1977.
47. A.J. Shearer, "An Evaluation of a Locally Homogeneous Model of Spray Evaporation," Ph.D. Thesis, Department of Mechanical Engineering, The Pennsylvania State University, University Park, PA, June, 1979.
48. C-P. Mao, "A Locally Homogeneous Flow Model of Spray Combustion," M.S. Thesis, Department of Mechanical Engineering, The Pennsylvania State University, University Park, PA, in preparation.
49. G.A. Szekely, Jr., "Experimental Evaluation of a Locally Homogeneous Flow Spray Combustion Model," M.S. Thesis, Department of Mechanical Engineering, The Pennsylvania State University, University Park, PA, in preparation.

General References

50. D.B. Spalding, "Theory of Particle Combustion at High Pressures," ARS J, Vol. 29, pp. 828-835, 1959.
51. P.R. Wieber, "Calculated Temperature Histories of Vaporizing Droplets to the Critical Point," AIAA J, Vol. 1, No. 12, pp. 2764-2770, 1963.
52. T.A. Brzustowski, "Chemical and Physical Limits on Vapor-Phase Diffusion Flames of Droplets," Can. J. Chem. Engr., Vol. 43, pp. 30-35, 1965.
53. D.E. Rosner, "On Liquid Droplet Combustion at High Pressures," AIAA J, Vol. 5, No. 1, pp. 163-166, 1967.
54. R.J. Priem and M.F. Heidmann, "Propellant Vaporization as a Design Criterion for Rocket Engine Combustion Chambers," NASA Technical Report 12-67, 1960.
55. J.A. Manrique and G.L. Borman, "Calculations of Steady State Droplet Vaporization at High Ambient Pressures," Int. J. Heat Mass Transfer, Vol. 12, pp. 1081-1095, 1969.

56. M. Goldsmith and S.S. Penner, "On the Burning of Single Drops of Fuel in an Oxidizing Atmosphere," Jet Propulsion, Vol. 24, pp. 245-251, 1954.
57. J.M. Prausnitz and P.L. Chueh, Computer Calculations for High Pressure Vapor-Liquid Equilibria, Prentice-Hall, Englewood Cliffs, N.J., 1968.
58. J.W. Aldred and A. Williams, "The Burning Rates of Drops of n-Alkanes," Combustion and Flame, Vol. 10, pp. 396-398, 1966.
59. O.W. Dykema and S.A. Greene, "An Experimental Study of RP-1, UDMH and N_2H_4 Single Droplet Burning in Air and in Oxygen," Progress in Astronautics and Rocketry Series, Vol. 2, Academic Press, New York, pp. 299-324, 1960.
60. B.R. Lawver, "Some Observations on the Combustion of N_2H_4 Droplets," AIAA Paper No. 65-355, 1965.
61. B.R. Lawver, T.C. Kosvic and B.P. Breen, "Effects of Additives on the Combustion of Hydrazine," AFRPL-TR-67-288, Dynamic Science Corp., Monrovia, CA, 1968.
62. T.C. Kosvic and B.P. Breen, "Study of Additive Effects on Hydrazine Combustion and Combustion Instability at High Pressure," AFRPL-TR-69-12, Dynamic Science Corp., Monrovia, CA, 1969.
63. D.T. Harrje (ed.), "Liquid Propellant Rocket Combustion Instability," NASA SP-194, Washington, D.C., Chapt. 3 and 4, 1972.
64. F.A. Williams, Combustion Theory, Addison-Wesley, Reading, MA, Chapt. 10, 1965.
65. J.S. T'ien, "Oscillatory Burning of Solid Propellants, including Gas-Phase Time Lag," Comb. Sci. and Tech., Vol. 5, pp. 47-54, 1972.
66. A.C. Antoine, "Mechanism of Burning of Liquid Hydrazine," Eighth Symposium (International) on Combustion, Williams and Wilkins, Baltimore, pp. 1057-1059, 1962.
67. G.M. Faeth, "Monopropellant Droplet Burning at Low Reynolds Numbers," Combustion and Flame, Vol. 11, pp. 167-174, 1967.
68. G.M. Faeth, "Flame Zone Development of Monopropellant Droplets," Combustion and Flame, Vol. 12, pp. 411-416, 1968.
69. G.M. Faeth, "Prediction of Pure Monopropellant Droplet Life Histories," AIAA J, Vol. 8, pp. 1308-1314, 1970.

70. J.G. Collier, Convective Boiling and Condensation, McGraw-Hill, London, 1972.
71. J.C. Weimer, G.M. Faeth and D.R. Olson, "Penetration of Vapor Jets Submerged in Subcooled Liquids," AIChE J, Vol. 19, pp. 552-558, 1973.
72. J.F. Avery and G.M. Faeth, "Combustion of a Submerged Gaseous Oxidizer Jet in a Liquid Metal," Fifteenth Symposium (International) on Combustion, The Combustion Institute, Pittsburgh, pp. 501-512, 1975.
73. Y. Oruma and M. Ogasawara, "Studies on the Structure of a Spray Combustion Flame," Fifteenth Symposium (International) on Combustion, The Combustion Institute, Pittsburgh, pp. 453-465, 1975.
74. J.A. Newman and T.A. Brzustowski, "Behavior of a Liquid Jet Near the Thermodynamic Critical Region," AIAA J, Vol. 9, pp. 1590-1602, 1971.
75. E.E. Khalil and J.H. Whitelaw, "Aerodynamic and Thermodynamic Characteristics of Kerosene-Spray Flames," Sixteenth Symposium (International) on Combustion, The Combustion Institute, Pittsburgh, pp. 569-576, 1977.
76. F.C. Lockwood and A.S. Naguib, "The Prediction of the Fluctuations in the Properties of Free, Round-Jet, Turbulent Diffusion Flames," Combustion and Flame, Vol. 24, pp. 109-124, 1975.
77. S. Corrsin and M.S. Uberoi, "Further Experiments on the Flow and Heat Transfer in a Heated Turbulent Air Jet," NASA Rept. No. 998, 1950.
78. I. Wygnanski and H.E. Fiedler, "Some Measurements in the Self-Preserving Jet," J. Fluid Mech., Vol. 38, pp. 577-612, 1969.
79. H.A. Becker, H.C. Hottel and G.C. Williams, "The Nozzle-Fluid Concentration Field of the Round, Turbulent, Free Jet," J. Fluid Mech., Vol. 30, pp. 285-303, 1967.
80. G. Hetsroni and M. Sokolov, "Distribution of Mass, Velocity and Intensity of Turbulence in a Two-Phase Turbulent Jet," Trans. ASME, J. Appl. Mech., Vol. 38, pp. 314-327, 1971.
81. S.R. Tross, "Characteristics of a Submerged Two-Phase Turbulent Free Jet," M.S. Thesis, Department of Mechanical Engineering, The Pennsylvania State University, University Park, PA, 1975.
82. S.V. Patankar and D.B. Spalding, Heat and Mass Transfer in Boundary Layers, 2nd Ed., Intertext Books, London, 1970.
83. S. Gordon and B.J. McBride, "Computer Program for Calculation of Complex Chemical Equilibrium Compositions, Rocket Performance, Incident and Reflected Shocks, and Chapman-Jouguet Detonations," NASA SP-273, Washington, 1971.